Journal of Molecular Spectroscopy 268 (2011) 199–210

Contents lists available at ScienceDirect

Journal of Molecular Spectroscopy

journal homepage: www.elsevier.com/locate/jms

A DPF data analysis yields accurate analytic potentials for $Li_2(a^3\Sigma_u^+)$ and $Li_2(1^3\Sigma_g^+)$ that incorporate 3-state mixing near the $1^3\Sigma_g^+$ state asymptote

Nikesh S. Dattani *, Robert J. Le Roy

Department of Chemistry, University of Waterloo, Waterloo, ON, Canada N2L 3G1

ARTICLE INFO

Article history:
Available online 8 May 2011

Keywords:
Direct potential fit
Lithium dimer
Resonance dipole interaction
Diatomic potential
Interstate coupling
Ultra-cold atoms
Morse/long-range (MLR) potential

ABSTRACT

A combined-isotopologue direct-potential-fit (DPF) analysis of optical and photoassociation spectroscopy data for the $a^3\Sigma_u^+$ and $1^3\Sigma_g^+$ states of Li_2 has yielded accurate analytic potential energy functions for both states. The recommended $M3LR_{5.3}^{8.0}(3)$ potential for the $a^3\Sigma_u^+$ state of $^{7,7}Li_2$ has a well depth of $\mathfrak{D}_e = 333.758(7)\ cm^{-1}$ and an equilibrium distance of $r_e = 4.17005(3)$ Å, and the associated scattering lengths are $a_{SL} = -14.759(9)$ Å for $^{7,7}Li_2$ and $a_{SL} = -1906(50)$ Å for $^{6,6}Li_2$. In spite of a gap of more than 5200 cm^{-1} (between $v(1^3\Sigma_g^+) = 7$ and $v(1^3\Sigma_g^+) = 62$) for which there are no data, the DPF procedure can readily yield a $1^3\Sigma_g^+$ state potential energy function that accurately represents all of the available data and smoothly bridges this gap. For $^{7,7}Li_2$ our recommended $M3LR_{6.3}^{3.6}(9)$ potential has a well depth of $\mathfrak{D}_e = 7093.44(3)\ cm^{-1}$, an equilibrium distance of $r_e = 3.06514(9)$ Å, and its long-range tail is defined by the lowest energy eigenvalue of a 3×3 matrix which takes into account the 3-state mixing near its asymptote.

1. Introduction

Modern theoretical studies of ultra-cold atomic gases demand a very accurate knowledge of the potential energy curves (PECs) of the systems of interest. Since Li_2 is the second smallest uncharged stable homonuclear molecule, its chemical and physical properties are particularly interesting. In recent years, considerable effort has been focussed on the lowest singlet states of Li_2 [1–10]. However, the properties of the triplet states of Li_2 are much less well known.

The first observation of discrete spectra involving the lowest triplet state of Li_2 was reported in 1985 by Xie and Field [11], who used perturbation-facilitated optical–optical double resonance (PFOODR) techniques to excite $2^3\Pi_g - a^3\Sigma_u^+$ emission. They observed transitions into $v(a^3\Sigma_u^+) = 0$–6, but because of the limited resolution available at the time, their results have been superseded by later work. The first high-resolution triplet-system measurements were reported in 1988 by Martin et al. [12], who performed a Fourier transform study of the $1^3\Sigma_g^+ \rightarrow a^3\Sigma_u^+$ system of $^{7,7}Li_2$ involving $v(1^3\Sigma_g^+) = 1$–7 of the upper state and $v(a^3\Sigma_u^+) = 0$–7 of the ground triplet state, with average measurement uncertainties of only ±0.01 cm^{-1}. Analogous results for the same system of $^{6,6}Li_2$, spanning the same ranges of vibrational levels, and with the same accuracy, were reported in 1989 by Linton et al. [13]. In 1999 Linton et al. reported [14] a high-resolution version of the PFOODR experiment of Xie and Field [11] which yielded observations (with uncertainties ranging from 0.005 to 0.01 cm^{-1}) of transitions into $v(a^3\Sigma_u^+) = 0$–9 from just over a dozen rotational levels of $v(2^3\Pi_g) = 1$ and 2. In addition, a two-photon photoassociation spectroscopy (PAS) experiment by Abraham et al. [15] had yielded a direct measurement of the 0.4160 (±0.0013) cm^{-1} binding energy of the $v = 10$, $N = 0$ level of the $a^3\Sigma_u^+$ state of $^{7,7}Li_2$.

In addition to the seven vibrational levels $v = 1$–7 of the $1^3\Sigma_g^+$ state observed in the emission experiments, the binding energies of levels $v = 62$–90 of $^{7,7}Li_2$ and $v = 56 - 84$ of $^{6,6}Li_2$ were measured in a PAS study by Abraham et al. in 1995 [16]. However, to date there has been no reported attempt to bridge the gap of more than 5000 cm^{-1} between these two sets of results in order to provide a global description of this state. This problem is illustrated by Fig. 1, which shows the regions of the $a^3\Sigma_u^+$ and $1^3\Sigma_g^+$ potentials associated with the data used in the present analysis (note that for $^{7,7}Li_2$, our final fits did not include the $v = 62$ datum, see Section 3.1 for details regarding the data used). The task of bridging the chasm for the $1^3\Sigma_g^+$ state is complicated by the fact that in the region very near its dissociation asymptote spanned by the PAS data, a transition from Hund's case (b) to case (c) coupling leads to a mixing of the $1^3\Sigma_g^+$ state with two other states that also have 1_g symmetry in this long-range ($r \gtrsim 20$ Å) region.

The only PECs which have been reported for the lowest triplet states ($a^3\Sigma_u^+$ and $1^3\Sigma_g^+$) of Li_2, are point-wise, semiclassical RKR curves generated from Dunham or near-dissociation expansions for the vibrational energies and B_v (inertial rotation) constants [12–14]. For the $1^3\Sigma_g^+$ upper state, those PECs were based only on data for vibrational levels $v(1^3\Sigma_g^+) = 1$–7 [12,13], since that

* Corresponding author. Address: Quantum Information Processing Building, Department of Materials, 12/13 Parks Road, Oxford OX1 3PH, UK.
E-mail addresses: dattani.nike@gmail.com (N.S. Dattani), leroy@uwaterloo.ca (R.J. Le Roy).

0022-2852/$ - see front matter © 2011 Elsevier Inc. All rights reserved.
doi:10.1016/j.jms.2011.03.030

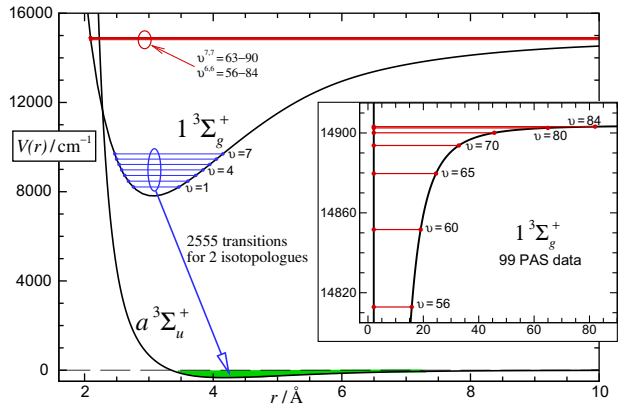

Fig. 1. Overview of the potential energy functions and observed vibrational levels of the $1^3\Sigma_g^+$ state associated with the present analysis. The inset shows a fragment of the $1^3\Sigma_g^+$ state potential at the energy range associated with the $^{6,6}Li_2$ PAS data. Not depicted in the diagram are the 137 transitions from the $2^3\Pi_g$ state to the $a^3\Sigma_u^+$ state, and the one PAS datum for the $a^3\Sigma_u^+$ state, that were also included in our analysis.

work preceded the photo-association spectroscopy (PAS) studies of this system [15,16]. Thus, the best available potential for the $1^3\Sigma_g^+$ state provides no realistic predictions for those subsequently observed high vibrational levels, took no account of interactions with other states of Li_2 near the dissociation asymptote of $1^3\Sigma_g^+$, and did not incorporate the theoretically known long-range behavior. Finally, in all studies of these states to date, $^{7,7}Li_2$ and $^{6,6}Li_2$ were treated independently, and as a consequence, the effect of Born-Oppenheimer breakdown (BOB) in this system remains unknown.

The present work presents a fully quantum mechanical direct-potential-fit (DPF) data analysis which considers all of the optical and PAS studies described above in terms of global analytic potential energy functions for the $a^3\Sigma_u^+$ and $1^3\Sigma_g^+$ states of Li_2, while independent term values are used to represent the 20 levels of the $2^3\Pi_g$ state giving rise to the observed high-resolution emission into $v(a^3\Sigma_u^+) = 0$—9. The three longest-range inverse-power contributions to the interaction energy are incorporated into the $a^3\Sigma_u^+$ and $1^3\Sigma_g^+$ state potential energy functions, and the function for the $1^3\Sigma_g^+$ state explicitly accounts for the three-state mixing mentioned in the previous paragraph. In addition, incorporation of adiabatic Born–Oppenheimer breakdown (BOB) correction functions in the hamiltonians for the $a^3\Sigma_u^+$ and $1^3\Sigma_g^+$ states allows the data for the two isotopologues to be treated simultaneously.

Three aspects of this system made its analysis unusually challenging. Firstly, the long-range tail of the $1^3\Sigma_g^+$ state PEC is not the familiar sum of simple inverse-power terms, since the $1^3\Sigma_g^+$ state couples strongly to two other states near the dissociation asymptote (see Section 2.3.1). Secondly, the fact that the leading long-range term of the PEC tail for the $1^3\Sigma_g^+$ state is C_3/r^3 means that the Morse/long-range (MLR) potential function leads to unphysical long-range behavior if not addressed appropriately (see Section 2.3.3) [10]. Finally, as illustrated by Fig. 1, the data for the $1^3\Sigma_g^+$ state has a gap between $v = 7$ and $v = 62$ for $^{7,7}Li_2$ and between $v = 7$ and $v = 56$ for $^{6,6}Li_2$. In both cases, these gaps span more than 70% of the corresponding well depths. Such a large gap in experimental information has never (to our knowledge) been treated successfully by a potential-fit analysis in a purely empirical manner.

2. Models and methodology

2.1. DPF data analyses and the radial hamiltonian

In a DPF spectroscopic data analysis, the upper and lower level of every observed transition is assumed to be an eigenvalue of an effective radial Schrödinger equation characterized by a parameterized potential energy function and (when appropriate) parameterized radial strength functions characterizing appropriate BOB correction terms. Given some plausible initial trial parameter values for characterizing the relevant potential, the solution of the associated Schrödinger equation yields an eigenvalue E_{vJ} and eigenfunction $\psi_{vJ}(r)$ for each observed level. The difference between the energies of appropriate upper and lower levels then yields an estimate of each observed transition energy, while use of the Hellmann–Feynman theorem:

$$\frac{\partial E_{vJ}}{\partial p_j} = \left\langle \psi_{vJ}(r) \left| \frac{\partial \widehat{H}}{\partial p_j} \right| \psi_{vJ}(r) \right\rangle, \tag{1}$$

yields the partial derivatives required for performing a least-squares fit of the simulated transitions of the experimental data.

Since the transition energies are not in general linear functions of the parameters defining the effective radial hamiltonian, a DPF analysis often requires the use of an iterative non-linear least-squares fitting procedure. The quality of a given fit is characterized by the value of the dimensionless root-mean-square deviation of the N_{data} experimental data (each of which is denoted by $y_{obs}(i)$) from the predicted values $y_{calc}(i)$ generated from the relevant hamiltonian(s):

$$\overline{dd} \equiv \sqrt{\frac{1}{N_{data}} \sum_{i=1}^{N_{data}} \left(\frac{y_{calc}(i) - y_{obs}(i)}{u(i)} \right)^2}, \tag{2}$$

in which $u(i)$ is the uncertainty in the reported value of experimental datum i. In the present work, these fits were performed using the publicly available program `DPotFit` [17], while the requisite initial estimates of the potential function parameters were obtained by applying the publicly available program `betaFIT` [18] to a preliminary set of RKR potential points generated using conventional Dunham expansions.

As with most diatomic DPF analyses reported to date, the present work is based on the effective radial Schrödinger equation presented by Watson [19,20], and uses the conventions described in Refs. [21,22]. In particular, the rovibrational levels of isotopologue α of diatomic molecule AB in a given electronic state are the eigenvalues of the radial Schrödinger equation:

$$\left(-\frac{\hbar^2}{2\mu_\alpha} \frac{d^2}{dr^2} + \left(V_{ad}^{(1)}(r) + \Delta V_{ad}^{(\alpha)}(r) \right) + \frac{\hbar^2 J(J+1)}{2\mu_\alpha r^2} \left(1 + g^{(\alpha)}(r)\right) \right) \psi_{vJ}(r) = E_{vJ} \psi_{vJ}(r), \tag{3}$$

in which $V_{ad}^{(1)}(r)$ is the effective adiabatic internuclear potential for a selected reference isotopologue labeled $\alpha = 1$, $\Delta V_{ad}^{(\alpha)}(r) = V_{ad}^{(\alpha)}(r) - V_{ad}^{(1)}(r)$ is the *difference* between the effective adiabatic potentials for isotopologue–α and isotopologue–1, $g^{(\alpha)}(r)$ is the non-adiabatic centrifugal potential correction function for isotopologue–α, and the reduced mass μ_α is defined by the atomic masses $M_A^{(\alpha)}$ and $M_B^{(\alpha)}$. Following standard conventions [19–23], the BOB correction terms $\Delta V_{ad}^{(\alpha)}(r)$ and $g^{(\alpha)}(r)$ are both written as a sum of contributions from component atoms A and B:

$$\Delta V_{ad}^{(\alpha)}(r) = \frac{\Delta M_A^{(\alpha)}}{M_A^{(\alpha)}} \widetilde{S}_{ad}^{A}(r) + \frac{\Delta M_B^{(\alpha)}}{M_B^{(\alpha)}} \widetilde{S}_{ad}^{B}(r), \qquad \text{and} \tag{4}$$

$$g^{(\alpha)}(r) = \frac{M_A^{(1)}}{M_A^{(\alpha)}} \widetilde{R}_{na}^{A}(r) + \frac{M_B^{(1)}}{M_B^{(\alpha)}} \widetilde{R}_{na}^{B}(r). \tag{5}$$

Here $\Delta M_{A/B}^{(\alpha)} = M_{A/B}^{(\alpha)} - M_{A/B}^{(1)}$ are the differences between the atomic masses of atoms A or B in isotopologue–α and in isotopologue–1. In the present case A = B = Li, and these expressions collapse to

$$\Delta V_{\rm ad}^{(\alpha)}(r) = \left(\frac{\Delta M_{\rm Li}^{(\alpha)}}{M_{\rm Li}^{(\alpha)}} + \frac{\Delta M_{\rm Li}^{(\alpha)}}{M_{\rm Li}^{(\alpha)}}\right) \widetilde{S}_{\rm ad}^{\rm Li}(r), \qquad \text{and} \tag{6}$$

$$g^{(\alpha)}(r) = \left(\frac{M_{\rm Li}^{(1)}}{M_{\rm Li}^{(\alpha)}} + \frac{M_{\rm Li}^{(1)}}{M_{\rm Li}^{(\alpha)}}\right) \widetilde{R}_{\rm na}^{\rm Li}(r). \tag{7}$$

Although only a single radial strength function of each type must be considered in the present case ($\widetilde{S}_{\rm ad}^{\rm Li}(r)$ and $\widetilde{R}_{\rm na}^{\rm Li}(r)$), both mass factors (one for Li^a and one for Li^b) must be retained in order to allow us to describe all possible molecular isotopologues.

2.2. The 'Basic' Morse/long-range (MLR) potential energy function

The next step is to introduce a function for representing the effective adiabatic internuclear potential for the reference isotopologue, $V_{\rm ad}^{(1)}(r) \equiv V(r)$. The present work is based on use of the extended Morse/long-range (MLR) potential energy function of Refs. [10,24],

$$V_{\rm MLR}(r) = \mathfrak{D}_e\left(1 - \frac{u_{\rm LR}(r)}{u_{\rm LR}(r_e)} e^{-\beta(r)\cdot y_p^{\rm eq}(r)}\right)^2, \tag{8}$$

in which $\mathfrak{D}_e$ is the well depth, r_e is the equilibrium internuclear distance, and the radial variable in the exponent is

$$y_p^{\rm eq}(r) \equiv \frac{r^p - r_e^p}{r^p + r_e^p}. \tag{9}$$

The function $\beta(r)$, which accounts for details of the potential's shape, is defined so that

$$\lim_{r\to\infty} \beta(r) \equiv \beta_\infty = \ln\left(\frac{2\mathfrak{D}_e}{u_{\rm LR}(r_e)}\right), \tag{10}$$

and as a result, the long-range behavior of the potential energy function is defined by the function $u_{\rm LR}(r)$:

$$V_{\rm MLR}(r) \simeq \mathfrak{D}_e - u_{\rm LR}(r) + u_{\rm LR}(r)^2/4\mathfrak{D}_e + \cdots, \tag{11}$$

while the factor in the denominator $u_{\rm LR}(r_e)$ is simply the value of that long-range tail function evaluated at the equilibrium bond length.

The theory of long-range intermolecular forces shows us that in general, $u_{\rm LR}(r)$ may be written in the form

$$u_{\rm LR}(r) = \sum_{i=1}^{\rm last} D_{m_i}(r) \frac{C_{m_i}}{r^{m_i}}, \tag{12}$$

in which the powers m_i and coefficients C_{m_i} of the terms contributing to this sum are determined by the symmetry of the given electronic state of the molecule and the nature of the atoms to which the molecule dissociates [25–28], while the 'damping functions' $D_{m_i}(r)$ take account of the weakening of the interaction energies associated with these simple inverse-power terms due to the overlap of the electronic wavefunctions of the interacting atoms [29]. While most previous applications of the MLR potential function form omitted the $D_{m_i}(r)$ damping function factors, it was shown in Ref. [24] that in addition to providing a more realistic physical description of the long-range potential tail, their introduction improves the extrapolation behavior of the repulsive short-range potential wall, and when they are included, fewer parameters are required to achieve a given quality of fit to experimental data. In either case, the structure of Eq. (11) means that at large distances where $u_{\rm LR}(r) \gg u_{\rm LR}(r)^2/(4\mathfrak{D}_e)$, the long-range behavior of $V_{\rm MLR}$ can be controlled easily by appropriately defining $u_{\rm LR}(r)$.

Following Ref. [24], the present work uses a modification of the Douketis damping function form of [30]:

$$D_{m_i}^{{\rm DS}(s)}(r) = \left(1 - e^{-\left(\frac{b^{\rm ds}(s)\cdot\rho r}{m_i} + \frac{c^{\rm ds}(s)\cdot(\rho r)^2}{m_i}\right)}\right)^{m_i+s}, \tag{13}$$

with $s = -1$, where $b^{\rm ds}(s)$ and $c^{\rm ds}(s)$ are system-independent parameters with $b^{\rm ds}(-1) = 3.30$ and $c^{\rm ds}(-1) = 0.423$. For interacting atoms A and B, $\rho \equiv \rho_{\rm AB} = 2\rho_{\rm A}\rho_{\rm B}/(\rho_{\rm A} + \rho_{\rm B})$, in which $\rho_{\rm A} = \left(I_p^{\rm A}/I_p^{\rm H}\right)^{2/3}$ is defined in terms of the ratio of the ionization potential of atom A $\left(I_p^{\rm A}\right)$ to that of an H atom $\left(I_p^{\rm H}\right)$. Inclusion of these ($s = -1$) damping functions means that at very short distances: $V_{\rm MLR}(r) \propto 1/r^2$ [24]. Comparisons with *ab initio* results for illustrative chemical and Van der Waals interactions showed that this type of damping function yielded quite realistic MLR short-range extrapolation behavior [24], so this $D_{m_i}(r)$ form is adopted here.

In order to ensure that $\beta(r)$ in Eq. (8) satisfies Eq. (10), it is customary to write it as the constrained polynomial:

$$\beta(r) = \beta_p^q(r) \equiv y_p^{\rm ref}(r)\beta_\infty + (1 - y_p^{\rm ref}(r)) \sum_{i=0}^{N} \beta_i \cdot (y_q^{\rm ref}(r))^i. \tag{14}$$

This function is expressed in terms of $y_p^{\rm ref}(r)$ and $y_q^{\rm ref}(r)$, which are similar to $y_p^{\rm eq}(r)$, but are defined with respect to a different expansion center ($r_{\rm ref}$) and involve two different powers, p and q (the reasons for this structure are discussed in Ref. [10]):

$$y_p^{\rm ref}(r) \equiv \frac{r^p - r_{\rm ref}^p}{r^p + r_{\rm ref}^p} \quad \text{and} \quad y_q^{\rm ref}(r) \equiv \frac{r^q - r_{\rm ref}^q}{r^q + r_{\rm ref}^q}. \tag{15}$$

The asymptotic long-range behavior of the exponential term in Eq. (8) gives rise to additional inverse-power contributions to the long-range potential of Eq. (11), with the leading term being proportional to $1/r^{m_1+p}$ (see Supplementary material for the explicit asymptotic long-range form of the exponential term). This means that the power p must be greater than $(m_{\rm last} - m_1)$ if the long-range behavior of Eq. (12) is to be maintained. There is no analogous formal constraint on the value of q; however, experience suggests that its value should lie in the range $2 \lesssim q \leqslant p$ [10,24,31]. In early work with this potential function form, the radial variables in Eq. (14) were both defined as $y_p^{\rm eq}(r)$ of Eq. (9) (i.e., $r_{\rm ref} = r_e$ and $q = p$) [32–35]. However, it has since been shown that setting $r_{\rm ref} \neq r_e$ and/or $q < p$ can significantly reduce the number of β_i parameters required to describe a given data set accurately, and yields more stable functions whose β_i parameters have magnitudes commensurate with the ranges of the dependent and independent variables being represented [10,24,31].[1]

A second consideration associated with the use of the damping functions of Eq. (13) is their effect on the shape of the short-range repulsive potential wall of an MLR potential. As was pointed out in Ref. [24], the fact that the radial variables $y_{p/q}^{\rm ref}(r) \to -1$ as $r \to 0$ means that at very small distances: $V_{\rm MLR}(r) \propto (u_{\rm LR}(r))^2$. If damping functions are neglected (i.e., if Eq. (12) did not include the $D_{m_i}(r)$ functions), then the limiting short-range behavior of the potential energy function would be $V_{\rm MLR}(r) \propto 1/r^{2m_{\rm last}}$. For a typical two- or three-term $u_{\rm LR}(r)$ function, $m_{\rm last} = 8$ or 10, and the resulting $1/r^{16}$ or $1/r^{20}$ short-range repulsive wall behavior would be unphysically excessively steep. In the data-sensitive region of the potential well, this excessive growth rate would be compensated for by the behavior of the empirically determined function $\beta(r)$. However, the unphysical high-order r^{-16} or r^{-20} singular behavior would re-assert itself in the shorter-range extrapolation region.

[1] Prior to the introduction of $r_{\rm ref} \neq r_e$, the $\beta(r)$ polynomials for potentials based on data spanning a large fraction of the potential well often had coefficients, $\{\beta_i\}$, whose magnitudes were orders of magnitude larger than the ranges of both $y_p(r)$ and $\beta(r)$. For example, in MgH(X) [24], the coefficients of $\beta(r)$ were larger by factors of up to 10^7. This is a signature of a 'marginally stable' function.

In this paper, the label for particular MLR potential function models is written as $\mathrm{M}x\mathrm{LR}^{r_{\mathrm{ref}}}_{p,q}(N)$, in which x is the number of dispersion energy constants incorporated into $u_{\mathrm{LR}}(r)$, while p, q, r_{ref} and N are defined above. The 'basic' MLR model described above is used herein to describe the potential energy function for the $a^3\Sigma_u^+$ state of Li_2. However, some enhancements were required for treating the $1^3\Sigma_g^+$ state.

2.3. Modified MLR potential for the $1^3\Sigma_g^+$ state of Li_2

2.3.1. Incorporating interstate coupling into the MLR model

At a preliminary stage of the present work, the $1^3\Sigma_g^+$ state of Li_2 was represented by the 'basic' MLR function of Eqs. (8)–(15), in which $u_{\mathrm{LR}}(r)$ consisted of three terms, with $m_i \in \{3, 6, 8\}$. This model was able to provide an excellent fit to both the fluorescence data for $v(1^3\Sigma_g^+) = 1$—7 and the PAS data for $v(1^3\Sigma_g^+, {}^{7,7}\mathrm{Li}_2) = 62$—70 and $v(1^3\Sigma_g^+, {}^{6,6}\mathrm{Li}_2) = 56$—65, whose upper limits both correspond to binding energies of about 24 cm^{-1}. However, when PAS data for higher vibrational levels were included in the analysis, the quality of fit got progressively worse, and the discrepancies could not easily be removed simply by increasing the order of the polynomial $\beta(r)$. The reason for this increasing inability of the basic MLR model to account for levels lying very near dissociation is that the $1^3\Sigma_g^+$ state of Li_2 couples to the two other states near its dissociation asymptote.

This same type of problem was encountered in a recent study of the $A(^1\Sigma_u^+) - X(^1\Sigma_g^+)$ system of Li_2. In that case the $0_u^+(A^1\Sigma_u^+)$ state which goes to the $\mathrm{Li}(^2P_{1/2}) + \mathrm{Li}(^2S_{1/2})$ asymptote couples to the $0_u^+(b^3\Pi)$ state which goes to the higher $\mathrm{Li}(^2P_{3/2}) + \mathrm{Li}(^2S_{1/2})$ limit [36,37], and the energies of levels lying near dissociation could not be explained properly without taking account of the inter-state mixing. Fortunately, Aubert-Frécon and co-workers had derived an analytic description of those coupled states based on the eigenvalues of a 2×2 interaction matrix [5,37], and it was shown in Ref. [10] that an accurate potential for the $A^1\Sigma_u^+$ state could easily be made using an MLR with $u_{\mathrm{LR}}(r)$ defined as their expression for the lower energy eigenvalue.

Treatment of levels lying near the dissociation limit of the $1^3\Sigma_g^+$ state of Li_2 involves a similar problem; while it dissociates to the $\mathrm{Li}(^2P_{1/2}) + \mathrm{Li}(^2S_{1/2})$ limit, it couples to the $1_g(^1\Pi_g)$ and $1_g(^3\Pi_g)$ states which correlate with the higher $\mathrm{Li}(^2P_{3/2}) + \mathrm{Li}(^2S_{1/2})$ limit [36,37]. Since the $\mathrm{Li}(^2P)$ spin-orbit splitting is quite small (0.335338 cm^{-1}[38]), the interstate coupling only becomes important for levels lying relatively close to the dissociation limit. Fortunately, Aubert-Frécon and co-workers have studied this case too [37]. In particular, they presented expressions for the six independent elements of the symmetric 3×3 matrix that defines the long-range interaction energies for these three states (see Eqs. (10) of Ref. [37], or the Supplementary material to this article). Their matrix elements took into account the first-order resonance-dipole ($1/r^3$) term, the leading dispersion energy terms, and the exchange energy. If we neglect the exchange terms, keep only the first two ($m_i \in \{6, 8\}$) dispersion energy terms, set the zero of energy at the $1^3\Sigma_g^+$ state asymptote, make use of the symmetry relation for $m_1 = 3$,

$$C_3^{\Sigma} \equiv C_3^{^3\Sigma_g^+} = 2C_3^{^1\Pi_g} = -2C_3^{^3\Pi_g}, \tag{16}$$

and that for $m_2 = 6$,

$$C_6^{\Pi} \equiv C_6^{^1\Pi_g} = C_6^{^3\Pi_g}, \tag{17}$$

and define $C_{6,8}^{\Sigma} \equiv C_{6,8}^{^3\Sigma_g^+}$, their 3×3 long-range interaction matrix $\mathbf{M}_{\mathrm{LR}}$ becomes (see the Supplementary material to this article)

$$\mathbf{M}_{\mathrm{LR}} = \begin{pmatrix} -\frac{1}{3}\left(\frac{C_3^{\Sigma}}{r^3} + \frac{C_6^{\Sigma}+2C_6^{\Pi}}{r^6} + \frac{C_8^{\Sigma}+C_8^{^1\Pi_g}+C_8^{^3\Pi_g}}{r^8}\right) & \frac{\sqrt{2}}{3}\left(\frac{C_3^{\Sigma}}{r^3} + \frac{C_6^{\Sigma}-C_6^{\Pi}}{r^6} + \frac{2C_8^{\Sigma}-C_8^{^1\Pi_g}-C_8^{^3\Pi_g}}{2r^8}\right) & \frac{1}{\sqrt{6}}\left(\frac{C_3^{\Sigma}}{r^3} + \frac{C_8^{^1\Pi_g}-C_8^{^3\Pi_g}}{r^8}\right) \\ \frac{\sqrt{2}}{3}\left(\frac{C_3^{\Sigma}}{r^3} + \frac{C_6^{\Sigma}-C_6^{\Pi}}{r^6} + \frac{2C_8^{\Sigma}-C_8^{^1\Pi_g}-C_8^{^3\Pi_g}}{2r^8}\right) & -\frac{2}{3}\left(\frac{C_3^{\Sigma}}{r^3} + \frac{2C_6^{\Sigma}+C_6^{\Pi}}{2r^6} + \frac{4C_8^{\Sigma}+C_8^{^1\Pi_g}+C_8^{^3\Pi_g}}{4r^8}\right) + \Delta E & \frac{1}{2\sqrt{3}}\left(\frac{C_3^{\Sigma}}{r^3} + \frac{C_8^{^1\Pi_g}-C_8^{^3\Pi_g}}{r^8}\right) \\ \frac{1}{\sqrt{6}}\left(\frac{C_3^{\Sigma}}{r^3} + \frac{C_8^{^1\Pi_g}-C_8^{^3\Pi_g}}{r^8}\right) & \frac{1}{2\sqrt{3}}\left(\frac{C_3^{\Sigma}}{r^3} + \frac{C_8^{^1\Pi_g}-C_8^{^3\Pi_g}}{r^8}\right) & -\left(\frac{C_6^{\Pi}}{r^6} + \frac{C_8^{^1\Pi_g}+C_8^{^3\Pi_g}}{2r^8}\right) + \Delta E \end{pmatrix}, \tag{18}$$

in which ΔE is the accurately known (positive) spin-orbit splitting energy of $\mathrm{Li}(^2P)$ [38]. Note that in contrast with Ref. [37], the present formulation treats attractive C_m coefficients as positive, rather than negative quantities. Following the correlation scheme given by Movre and Pichler [36], the lowest energy eigenvalue of the matrix (18) defines the long-range tail of the $1^3\Sigma_g^+$ state interaction potential; see Fig. 2.

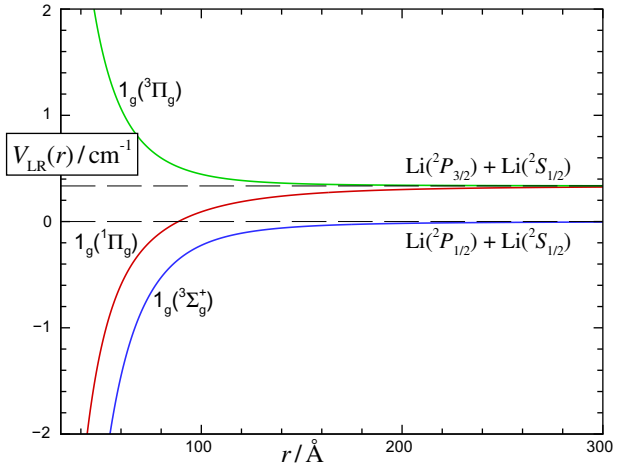

Fig. 2. Eigenvalues of Eq. (18) for the 1_g states of Li_2 dissociating to the $\mathrm{Li}(^2S) + \mathrm{Li}(^2P)$ limits, as generated using the long-range coefficients of Tang et al. [42].

Analytic expressions for the three eigenvalues of Eq. (18) were also reported in Ref. [37]. Those expressions were obtained by analytically solving for the zeros of the characteristic (cubic) polynomial for $\mathbf{M}_{\mathrm{LR}}$.[2] However, we do not recommend using their analytic expressions (see the discussion about their eigenvalue expressions in the Supplementary material). Kopp has demonstrated that when such formulas for the solutions to a cubic equation are evaluated numerically using double precision floating point arithmetic, the results might differ from the true values by more than 10^6 [40]. Moreover, the least squares fitting procedure used to optimize the parameters of the potential in order to give the most accurate

[2] This can be accomplished using formulas such as Eqs. (33) from Ref. [40]. Such formulas were first published by Gerolamo Cardano [39], but Scipione del Ferro and Niccolò Fontana Tartaglia discovered methods to solve cubic equations much earlier [52].

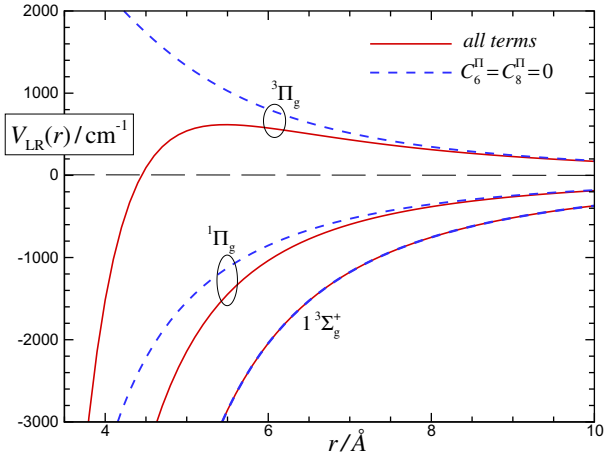

Fig. 3. Illustration of the effect of setting $C_6^{\Pi}=C_8^{^1\Pi_g}=C_8^{^3\Pi_g}=0$ in Eq. (18).

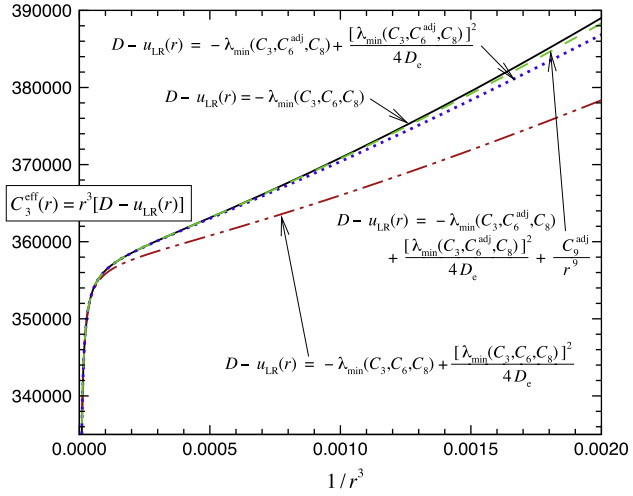

Fig. 4. Comparison of four representations of the long-range potential for the $1^3\Sigma_g^+$ state of Li_2, with energies in cm^{-1} and lengths in Å.

potential of a given form requires derivatives of the potential (and therefore, by the chain rule, requires derivatives of the lowest energy eigenvalue of $\mathbf{M}_{LR}$) with respect to all of the fitting parameters. The symbolic expressions for the derivatives of the lowest eigenvalue with respect to the fitting parameters required by the least-squares fitting procedure are inconveniently complicated. Because of these problems, in the present work the interaction matrix is diagonalized numerically (using the Jacobi diagonalization algorithm [40,41] which diagonalizes the matrix to practically machine precision), and the derivatives of the eigenvalues with respect to each fitting parameter p were computed using the discrete version of the Hellmann–Feynman theorem:

$$\frac{\partial\lambda_i}{\partial p}=\left\langle\phi_{\lambda_i}\left|\frac{\partial\mathbf{M}_{LR}}{\partial p}\right|\phi_{\lambda_i}\right\rangle, \tag{19}$$

in which λ_i is the appropriate eigenvalue of the $\mathbf{M}_{LR}$ matrix, and ϕ_{λ_i} is the corresponding eigenvector. A more detailed discussion that compares our numerical eigenvalues with the analytic expressions of Ref. [38] can be found in the Supplementary material.

2.3.2. Simplifying the treatment of interstate coupling for $Li_2(1^3\Sigma_g^+)$

The treatment of the long-range behavior of the $A^1\Sigma_u^+$ state of Li_2 presented in Ref. [10] was precisely analogous to that used here for the $1^3\Sigma_g^+$ state, except that while that case involved a 2×2 matrix whose eigenvalues were determined analytically, the present case involves the 3×3 matrix of Eq. (18) whose eigenvalues are calculated numerically. In the treatment of the $A^1\Sigma_u^+$ state, it was shown that the C_6^{Π}/r^6 and C_8^{Π}/r^8 terms had virtually no effect on the lower energy (Σ state) eigenvalue of the 2×2 long-range interstate coupling matrix. This led us to consider making the same simplification here.

Following the approach of Ref. [10], we compared the values of the lowest energy eigenvalue of Eq. (18) obtained when C_3^{Σ} and all $C_6^{\Sigma/\Pi}$ and $C_8^{\Sigma/\Pi}$ coefficients were defined by the theoretical values of Tang et al. [42], with those obtained after setting $C_6^{\Pi}=C_8^{^1\Pi_g}=C_8^{^3\Pi_g}=0$. Over the range $r=2$ to 500 Å, the difference between these two estimates of the lowest eigenvalue was always less than $3\times10^{-6}\,cm^{-1}$. Thus, it seems clear that in the present treatment of the $1^3\Sigma_g^+$ state of Li_2, no significant errors will be introduced if contributions involving C_6^{Π}, $C_8^{^1\Pi_g}$ and $C_8^{^3\Pi_g}$ are omitted from Eq. (18). At the same time, it is important to note that for small internuclear distances, these C_6^{Π} and C_8^{Π} coefficients *cannot* be neglected when using the two higher energy eigenvalues of Eq. (18) to define the long-range tails of the $^3\Pi_g$ and $^1\Pi_g$ states which couple with the $1^3\Sigma_g^+$ state of interest here. This point is illustrated by Fig. 3, which compares plots of the three eigenvalues of Eq. (18) obtained using all of the $C_n^{\Sigma/\Pi}$ coefficients of Tang et al. [42] (solid red curves[3]) with those obtained from this same matrix when $C_6^{\Pi}=C_8^{^1\Pi_g}=C_8^{^3\Pi_g}=0$ (dashed blue curves). It is clear from Fig. 3, that at the smaller distances where the C_6 and C_8 terms become important, one cannot use the above approximation when calculating the eigenvalues of Eq. (18) associated with the two Π_g states.[4] This argument for the justification of this simplification is unaffected by the following two changes made (in Sections 2.3.3 and 2.3.4), and the Supplementary material contains tests to demonstrate this.

2.3.3. Implications of the quadratic term in the MLR potential function form

It was shown in Ref. [10] that contributions from the quadratic term in Eq. (11) can give rise to spurious changes in the long-range behavior of the MLR potential function form. In the present case, the leading terms in the long-range potential for the $1^3\Sigma_g^+$ state of Li_2 correspond to $m_i\in\{3,6,8\}$. If we temporarily ignore the effects of damping and interstate coupling in order to write $u_{LR}(r)$ as a simple inverse-power sum, the presence of the quadratic term in Eqs. (8) and (11) mean that the effective long-range behavior of the MLR potential would be

$$V_{MLR}(r)\simeq\mathfrak{D}_e-\frac{C_3}{r^3}-\frac{C_6}{r^6}-\frac{C_8}{r^8}+\frac{(C_3)^2/(4\mathfrak{D}_e)}{r^6}+\frac{C_3C_6/(2\mathfrak{D}_e)}{r^9}+\cdots. \tag{20}$$

Thus, if the overall effective long-range behavior is to be defined by an inverse-power sum governed by the specified C_3, C_6 and C_8 coefficients (and *not* include the last two terms in Eq. (20)), the definition of $u_{LR}(r)$ must compensate for the quadratic terms by being defined as

$$u_{LR}(r)=\frac{C_3}{r^3}+\frac{C_6^{adj}}{r^6}+\frac{C_8}{r^8}+\frac{C_9^{adj}}{r^9}, \tag{21}$$

in which $C_6^{adj}\equiv C_6+(C_3)^2/(4\mathfrak{D}_e)$ and $C_9^{adj}\equiv C_3C_6^{adj}/(2\mathfrak{D}_e)$.

Since the long-range tail of our $1^3\Sigma_g^+$ state potential also includes interstate coupling, these expressions for C_6^{adj} and C_9^{adj} (which were derived analytically for potentials with simpler long-range tails) need to be tested in order to ascertain that they do indeed cancel the effect of the spurious last two terms shown

[3] For interpretation of color in Figs. 1–9, the reader is referred to the web version of this article.

[4] Similarly, leaving $C_{6,8}^{\Pi}$ at the theoretical values and setting $C_{6,8}^{\Sigma}=0$ has little effect on the solid curves for the $^3\Pi_g$ and $^1\Pi_g$ states, but the resulting plot for the $1^3\Sigma_g^+$ state deviates significantly from its corresponding solid and dashed curves in Fig. 3.

in Eq. (20). Results of a numerical test of this question are presented in Fig. 4, which displays plots of the quantity $C_3^{\rm eff}(r) \equiv r^3(\mathfrak{D} - u_{\rm LR}(r))$ *vs.* r^{-3} for three different definitions of $u_{\rm LR}(r)$. This type of plot illustrates the nature of the long-range interaction on a reduced scale. If $u_{\rm LR}(r)$ was defined as the simple inverse-power sum of Eq. (21), as $r^{-3} \to 0$ the resulting plot would approach an intercept of C_3 with a limiting slope of $C_6^{\rm eff}$ [32]. In the present case, however, the mixing of three states near the potential's dissociation asymptote causes all of the plots in Fig. 4 to drop off sharply for $r^{-3} \lesssim 10^{-4}$ Å^{-3}.

As mentioned in Section 2.3.1, the desired long-range behavior is achieved when $u_{\rm LR}(r)$ is defined simply as the lowest energy eigenvalue of the matrix of Eq. (18), $u_{\rm LR}(r) = -\lambda_{\rm min}(r)$. This desired behavior is defined by the solid black curve in Fig. 4. The dash-dot-dot red curve in Fig. 4 then shows how the long-range behavior of the associated MLR potential, which includes the quadratic term of Eq. (11), deviates from this desired long-range behavior. Next, the dotted blue curve shows the effect on the long-range MLR behavior, of replacing C_6^{Σ} by the quantity $C_6^{\rm adj}$ defined above. It is immediately clear that this removes most of the discrepancy with the 'ideal' long-range behavior (the solid black curve). Finally, the dashed green curve shows the effect on the long-range MLR potential tail, of also including the $C_9^{\rm adj}/r^9$ term in (21) in order to cancel out the spurious r^{-9} term in Eq. (20). It is clear that use of the resulting definition

$$u_{\rm LR}(r) = -\lambda_{\rm min}\left(C_3, C_6^{\rm adj}, C_8; r\right) + C_9^{\rm adj}/r^9, \tag{22}$$

brings the long-range tail of the overall MLR potential function into practically exact agreement with the desired form. This remains true whether or not the simplification of the last section (Section 2.3.2) is made and whether or not the inclusion of retardation (described in the next section) is made. The Supplementary material contains tests to demonstrate this.

2.3.4. Inclusion of retardation in the model potential for $Li_2(1^3\Sigma_g^+)$

It has been known for a long time that at the very large distances, where the C_3/r^3 term comes to dominate the interaction energy in this type of system, 'retardation' effects due to the finite speed of light should not be neglected [43,44]. It was shown by Meath [44] that the effect of retardation on an s/p resonance-dipole interaction can be accounted for by multiplying C_3^{Σ} by the function $f_{\rm ret}^{\Sigma}(r)$ and C_3^{Π} by the function $f_{\rm ret}^{\Pi}(r)$, where

$$f_{\rm ret}^{\Sigma} = \cos\left(\frac{r}{\lambda\!\!\!^{-}_{SP}}\right) + \left(\frac{r}{\lambda\!\!\!^{-}_{SP}}\right)\sin\left(\frac{r}{\lambda\!\!\!^{-}_{SP}}\right), \tag{23}$$

$$f_{\rm ret}^{\Pi} = f_{\rm ret}^{\Sigma} - \left(\frac{r}{\lambda\!\!\!^{-}_{SP}}\right)^2\cos\left(\frac{r}{\lambda\!\!\!^{-}_{SP}}\right), \tag{24}$$

in which $\lambda\!\!\!^{-}_{SP} = \lambda_{SP}/2\pi$ and λ_{SP} is the wavelength of light associated with the atomic $^2S - {}^2P$ transition, which for ^{7}Li is implicitly given in Table 2, and for ^{6}Li is given in the analogous table for $^{6,6}Li_2$ in the Supplementary material.

It is a straightforward matter to incorporate this retardation behavior into the MLR potential function form. In particular, on setting $C_6^{\Pi} = C_8^{\Pi} = 0$, making use of the symmetry relationships of Eq. (16) for the $C_3^{\Sigma}, C_3^{^1\Pi_g}$ and $C_3^{^3\Pi_g}$ coefficients, and replacing C_6^{Σ} by $C_6^{\Sigma,{\rm adj}}$, the long-range interstate coupling matrix for the three 1_g states dissociating to yield $Li(^2P) + Li(^2S_{1/2})$ becomes

$$\mathbf{M}_{\rm LR}^{\rm ret} = \begin{pmatrix} -\frac{1}{3}\left(\frac{C_3^{\Sigma} f_{\rm ret}^{\Sigma}}{r^3} + \frac{C_6^{\Sigma,{\rm adj}}}{r^6} + \frac{C_8^{\Sigma}}{r^8}\right) & \frac{\sqrt{2}}{3}\left(\frac{C_3^{\Sigma} f_{\rm ret}^{\Sigma}}{r^3} + \frac{C_6^{\Sigma,{\rm adj}}}{r^6} + \frac{C_8^{\Sigma}}{r^8}\right) & \frac{1}{\sqrt{6}}\frac{C_3^{\Sigma} f_{\rm ret}^{\Pi}}{r^3} \\ \frac{\sqrt{2}}{3}\left(\frac{C_3^{\Sigma} f_{\rm ret}^{\Sigma}}{r^3} + \frac{C_6^{\Sigma,{\rm adj}}}{r^6} + \frac{C_8^{\Sigma}}{r^8}\right) & -\frac{2}{3}\left(\frac{C_3^{\Sigma} f_{\rm ret}^{\Sigma}}{r^3} + \frac{C_6^{\Sigma,{\rm adj}}}{r^6} + \frac{C_8^{\Sigma}}{r^8}\right) + \Delta E & \frac{1}{2\sqrt{3}}\frac{C_3^{\Sigma} f_{\rm ret}^{\Pi}}{r^3} \\ \frac{1}{\sqrt{6}}\frac{C_3^{\Sigma} f_{\rm ret}^{\Pi}}{r^3} & \frac{1}{2\sqrt{3}}\frac{C_3^{\Sigma} f_{\rm ret}^{\Pi}}{r^3} & \Delta E \end{pmatrix}. \tag{25}$$

Unless stated otherwise, the definition of the long-range tail of the MLR potential for the $1^3\Sigma_g^+$ used throughout the rest of this study is therefore given by

$$u_{\rm LR}(r) \equiv -\lambda_{\rm min}^{\rm ret}\left(C_3^{\Sigma}, C_6^{\rm adj}, C_8^{\Sigma}; r\right) + C_9^{\rm adj}/r^9 \tag{26}$$

in which $\lambda_{\rm min}^{\rm ret}\left(C_3^{\Sigma},\ C_6^{\rm adj},\ C_8^{\Sigma}; r\right)$ is the lowest energy eigenvalue of the interaction energy matrix of Eq. (25).

2.4. Born–Oppenheimer breakdown functions

The radial strength functions in Eqs. (6) and (7) may be written as polynomials constrained to have specified asymptotic values using the format of Eq. (14)

$$\widetilde{S}_{\rm ad}^{\rm Li}(r) = y_{p_{\rm ad}}^{\rm eq}(r)u_{\infty}^{\rm Li} + (1 - y_{p_{\rm ad}}^{\rm eq}(r))\sum_{i=0} u_i^{\rm Li}\cdot(y_{q_{\rm ad}}^{\rm eq}(r))^i, \qquad \text{and} \tag{27}$$

$$\widetilde{R}_{\rm na}^{\rm Li}(r) = y_{p_{\rm na}}^{\rm eq}(r)t_{\infty}^{\rm Li} + (1 - y_{p_{\rm na}}^{\rm eq}(r))\sum_{i=0} t_i^{\rm Li}\cdot(y_{q_{\rm na}}^{\rm eq}(r))^i, \tag{28}$$

in which $u_{\infty}^{\rm Li}$ and $t_{\infty}^{\rm Li}$ are the values of these functions in the limit $r \to \infty$, $u_0^{\rm Li}$ and $t_0^{\rm Li}$ define their values at $r = r_e$, and the radial variables are versions of Eq. (9) associated with chosen values of the integers $p_{\rm ad}$, $p_{\rm na}$, $q_{\rm ad}$ and $q_{\rm na}$. The discussion of Ref. [22] shows that $t_{\infty}^{\rm A,B} = 0.0$ for any molecule which dissociates to yield uncharged atoms, so $t_{\infty}^{\rm Li}(a^3\Sigma_u^+) = t_{\infty}^{\rm Li}(1^3\Sigma_g^+) = 0.0$. In addition, we adopt the Watson convention of setting the parameter $t_0^{\rm Li} = 0.0$ for both the $a^3\Sigma_u^+$ and $1^3\Sigma_g^+$ states, since its value cannot be determined from transition-frequency data alone [19,20,22].

Neglecting hyperfine splittings, the absolute zero of energy is defined as the energy of ground-state atoms separated at $r \to \infty$ [21], so by definition, $u_{\infty}^{\rm Li}(a^3\Sigma_u^+) = 0.0$.[5] Since the $1^3\Sigma_g^+$ state of Li_2 dissociates to one ground-state ($^2S_{1/2}$) and one excited-state ($^2P_{1/2}$) atom, the value of $u_{\infty}^{\rm Li}(1^3\Sigma_g^+)$ is then defined in terms of the difference between the atomic $^2P_{1/2} \leftarrow {}^2S_{1/2}$ excitation energies for ^{6}Li and ^{7}Li, which is [21,38]

$$\begin{aligned}\delta E_{7Li}^{6Li}(^2P_{1/2}) &= \Delta E^{6Li}(^2P_{1/2} \leftarrow {}^2S_{1/2}) - \Delta E^{7Li}(^2P_{1/2} \leftarrow {}^2S_{1/2}) \\ &= -0.351338\ {\rm cm}^{-1}.\end{aligned} \tag{29}$$

This is the difference between the energy asymptotes of the $1^3\Sigma_g^+$ states of $^{6,6}Li_2$ and $^{7,7}Li_2$, and it defines the asymptotic value of the adiabatic radial strength function for the $1^3\Sigma_g^+$ state [21]. Since we select $^{7,7}Li_2$ as the reference isotopologue, this yields

$$u_{\infty}^{\rm Li}\left(1^3\Sigma_g^+\right) = \delta E_{7Li}^{6Li}(^2P_{1/2})/2\left(1 - \frac{M(^7{\rm Li})}{M(^6{\rm Li})}\right) = 1.05574\ {\rm cm}^{-1}. \tag{30}$$

We now address the choice of powers $p_{\rm ad}$, $q_{\rm ad}$, $p_{\rm na}$ and $q_{\rm na}$ for defining the radial expansion variables in Eqs. (27) and (28). As was pointed out in Ref. [21], if the effective adiabatic potential for the 'minor' isotopologue is to have the same limiting long-range behavior as that for the reference isotopologue, $p_{\rm ad}$ must be greater than or equal to the power of the longest-range term in the intermolecular potential for that state. Thus, we set $p_{\rm ad}(a^3\Sigma_g^+) = 6$ and $p_{\rm ad}(1^3\Sigma_g^+) = 3$. Note that these BOB correction radial strength functions are relatively weak (strength $\sim 1 - 2$ cm^{-1}) and slowly varying, and few terms are required to define them. As a result, there is no need here to introduce an $r_{\rm ref} \neq r_e$ extension into the definition of the expansion variables in Eqs. (27) and (28), and for the sake of simplicity we set $q_{\rm ad}(a^3\Sigma_u^+) = p_{\rm ad}(a^3\Sigma_u^+) = 6$ and $q_{\rm ad}(1^3\Sigma_g^+) = p_{\rm ad}(1^3\Sigma_g^+) = 3$.

We are not aware of any theoretical predictions regarding the limiting long-range behavior of the centrifugal non-adiabatic radial

[5] This neglect of hyperfine effects is justified by the fact that the binding energy of the highest observed level $v(a^3\Sigma_u^+, {}^{7,7}Li_2) = 10$ is more than an order of magnitude larger than the hyperfine intereaction energy, which is about 0.027 cm^{-1} [15,38].

Table 1
Summary of experimental data used in the present work. A listing of all of the experimental data, and a list of the 13 'outliers' excluded from our analysis is available in the Supplementary material to this article.

Isotop.	Type	unc. (cm^{-1})	$v(2^3\Pi_g)$	$v(1^3\Sigma_g^+)$	$v(a^3\Sigma_u^+)$	#Data	Source
$^{7,7}Li_2$	$1^3\Sigma_g^+$ emission	0.01	–	1–7	0–7	1279	Ref. [12]
	$2^3\Pi_g$ emission	0.005–0.01	1–2	–	0–9	137	Ref. [14]
	PAS($1^3\Sigma_g^+$)	0.0043–0.00073	–	63–90	–	30	Ref. [16]
	PAS($a^3\Sigma_u^+$)	0.0013	–	–	10	1	Ref. [15]
$^{6,6}Li_2$	$1^3\Sigma_g^+$ emission	0.01	–	1–7	0–7	1276	Ref. [13]
	PAS($1^3\Sigma_g^+$)	0.00110–0.01067	–	56–84	–	69	Ref. [16]
	Overall		1–2	1–90	0–10	2792	

strength function $\widetilde{R}_{na}^{A/B}(r)$ (see Eq. (5)), so we have no basis for assigning particular values to p_{na}. Moreover, as is true for the analogous q parameters in Eqs. (14), (27) and (28), the value of q_{na} has no effect on the limiting long-range behavior of $\widetilde{R}_{na}^{A/B}(r)$, so there are no constraints on its value. At the same time, Fig. 3 of Ref. [22] shows that use of too small values for these powers can give rise to physically implausible features in the resulting functions on the interval between the data region and the asymptote, while use of too high values tends to require an excessive number of polynomial coefficients. For simplicity, we therefore chose, for both electronic states, $p_{na} = q_{na} = 3$ in fits to models which included non-zero $\widetilde{R}_{na}^{Li}(r)$ functions.

The difference between the well depths of two Li isotopologues can be written as the difference between the right hand sides of $\mathfrak{D}_e^{(\alpha)} \equiv V_{ad}^{(\alpha)}(r=\infty) - V_{ad}^{(\alpha)}(r=r_e)$, and $\mathfrak{D}_e^{(1)} \equiv V_{ad}^{(1)}(r=\infty) - V_{ad}^{(1)}(r=r_e)$. The resultant expression can then be rearranged and then rewritten using the denition of $\Delta V_{ad}^{(\alpha)}(r)$ to give:

$$\delta\mathfrak{D}_e^{(\alpha)} \equiv \mathfrak{D}_e^{(\alpha)} - \mathfrak{D}_e^{(1)} = \Delta V_{ad}^{(\alpha)}(r=\infty) - \Delta V_{ad}^{(\alpha)}(r=r_e). \tag{31}$$

Since $y_{p_{ad}}^{ref}(r_e) = 0$ and $y_{p_{ad}}^{ref}(r \to \infty) = 1$, the algebraic forms of Eqs. (31), (6) and (27) mean that the difference between the well depths of different Li_2 isotopologues in a given electronic state is given by the expression [22]

$$\delta\mathfrak{D}_e^{(\alpha)} = \mathfrak{D}_e^{(\alpha)} - \mathfrak{D}_e^{(1)} = \left(\frac{\Delta M_{Li^a}^{(\alpha)}}{M_{Li^a}^{(\alpha)}} + \frac{\Delta M_{Li^b}^{(\alpha)}}{M_{Li^b}^{(\alpha)}}\right)\left(u_\infty^{Li} - u_0^{Li}\right). \tag{32}$$

The analogous shift in the equilibrium distance r_e is [10]

$$\delta r_e^{(\alpha)} = r_e^{(\alpha)} - r_e^{(1)} = -\left(\frac{\Delta M_{Li^a}^{(\alpha)}}{M_{Li^a}^{(\alpha)}} + \frac{\Delta M_{Li^b}^{(\alpha)}}{M_{Li^b}^{(\alpha)}}\right)\frac{\widetilde{S}'_{ad}(r_e)}{\bar{k}}, \tag{33}$$

in which $\bar{k}$ is the harmonic force constant at the potential minimum in units cm^{-1} Å^{-2}, and

$$\widetilde{S}'_{ad}(r_e) \equiv \left(\frac{d\widetilde{S}_{ad}}{dr}\right)_{r=r_e} = \frac{(u_\infty - u_0)p_{ad} + u_1 q_{ad}}{2r_e}. \tag{34}$$

Here, $\mathfrak{D}_e^{(1)}$ and $r_e^{(1)}$ are the well depth and equilibrium distance of the MLR potential for the chosen reference isotopologue (here $^{7,7}Li_2$), and are parameters explicitly determined by the DPF analysis. Similarly, by Eq. (10) in Ref. [22], the electronic isotope shift will be

$$\delta\left\{\Delta T_e^{(\alpha)}\right\} = \Delta T_e^{(\alpha)} - \Delta T_e^{(1)} = \left(\frac{\Delta M_{Li^a}^{(\alpha)}}{M_{Li^a}^{(\alpha)}} + \frac{\Delta M_{Li^b}^{(\alpha)}}{M_{Li^b}^{(\alpha)}}\right)\left(u_0^{Li}(1^3\Sigma_g^+) - u_0^{Li}(a^3\Sigma_u^+)\right). \tag{35}$$

Note that this use of Eqs. (30) and (32) is not valid for the mixed isotopologue $^{6,7}Li_2$, as it would cause its potential asymptote to lie at a fictitious point half way between the $^6Li(^2P_{1/2}) + {}^7Li(^2S_{1/2})$ and $^7Li(^2P_{1/2}) + {}^6Li(^2S_{1/2})$ limits. In our treatment of the analogous situation for the $A^1\Sigma_u^+$ state of Li_2, this problem was addressed by introducing an *ad hoc* correction term which caused the potential function for the mixed isotopologue to go to the correct (lower) limit [10]. However, as there are currently no $^{6,7}Li_2$ data for the $1^3\Sigma_g^+$ state it seems superfluous to introduce an analogous term here, and we merely note that energy levels and other properties for the $1^3\Sigma_g^+$ state of $^{6,7}Li_2$ predicted by the present model will become unreliable within $1-2\ cm^{-1}$ of the potential asymptote.

Finally, as was pointed out by McAlexander et al. [45], for the $1^3\Sigma_g^+$ state of Li_2, the dominant BOB contribution to the rotationless potential at large r has the form

$$\Delta V_{ad}^{(\alpha)}(r) \simeq 2B^{(\alpha)}(r) = 2\left(\frac{\hbar^2}{2\mu_\alpha r^2}\right), \tag{36}$$

and since μ_α for isotopic Li_2 is relatively small, this behavior must be considered. Following the approach of Refs. [45,46,10], we have chosen to treat this term as a separate additive contribution to the effective interaction potential for each isotopologue, which therefore has the form:

$$V_{ad,tot}^{(\alpha)}(r) = V_{MLR}(r) + \Delta V_{ad}^{(\alpha)}(r) + 2B^{(\alpha)}(r). \tag{37}$$

As was pointed out by Vogt et al. [46], this $\Delta V_{ad}(r)$ term is readily incorporated into the hamiltonian by simply replacing the factor $J(J+1)$ in Eq. (3) by $(J(J+1)+2)$, and their approach was adopted here. However, this means that the overall $1^3\Sigma_g^+$ state well depth and equilibrium distance are actually $\mathfrak{D}_e^{tot}(1^3\Sigma_g^+) = \mathfrak{D}_e^{(\alpha)} - 2B^{(\alpha)}(r_e)$ and $r_e^{tot}(1^3\Sigma_g^+) = r_e^{(\alpha)} + 4B^{(\alpha)}(r_e)/(\bar{k}r_e)$, where $\mathfrak{D}_e^{(\alpha)}$ and $r_e^{(\alpha)}$ are defined by Eqs. (32) and (33), and $\mathfrak{D}_e^{(1)}$ and $r_e^{(1)}$ are the (fitted) reference-isotopologue MLR parameters for that state.

3. Potentials for the $a^3\Sigma_u^+$ and $1^3\Sigma_g^+$ states of Li_2

3.1. Data set and methodology

An overview of the experimental data used in this work is presented in Table 1. Most of the data (2555 out of 2792 observations), came from fluorescence experiments performed by Martin et al. [12] and Linton et al. [13]. That data set, which extended up to $v = 7$ for both the $a^3\Sigma_u^+$ state and the $1^3\Sigma_g^+$ state, was enlarged by the inclusion of 137 $(2^3\Pi_g - a^3\Sigma_u^+)$ transitions of $^{7,7}Li_2$ taken from the study of Ref. [14], which extended the $a^3\Sigma_u^+$ vibrational range to $v = 9$. Finally, information about levels lying very near dissociation was provided by the one available PAS binding energy measurement for the $v = 10$ level of the $a^3\Sigma_u^+$ state [15], and 99 PAS data for very high levels of the $1^3\Sigma_g^+$ state [16][6]; hyperfine structure was not resolved for the former, while the latter were reported relative to the hyperfine centre of gravity. Throughout this study, the

[6] The PAS data for $v(^{7,7}Li_2) = 62$, $N = 1$, $v(^{6,6}Li_2) = 80$, $N = 1$ and $v(^{6,6}Li_2) = 68$, $N = 2$ appear to be outliers, and were omitted from the final analyses. A list of the 10 omitted fluorescence experiment data that appear as outliers is provided with the complete data set used in our analysis in the Supplementary material.

upper levels of all transitions originating in the $2^3\Pi_g$ state were represented by independent fitted term values. A listing of the experimental data used in the present analysis is included as Supplementary material.

All of the DPF data analysis fits described herein were performed using the program `DPotFit`, which is freely available (with a manual) online [17]. The initial trial values of the parameters β_i required for those fits were generated by applying the program `betaFIT` (also available online) [18] to sets of turning points obtained from preliminary versions of the analysis.

3.2. Model for $Li_2(a^3\Sigma_u^+)$

The $a^3\Sigma_u^+$ state of Li_2 dissociates to yield two S-state atoms, and ignoring hyperfine effects, there is no noteworthy interstate coupling. The theory of intermolecular forces therefore tells us that the leading contributions to the long-range intermolecular potential should consist of terms associated with inverse powers $m_i \in \{6, 8, 10\}$. The present analysis therefore represented the potential energy for this species by an MLR potential incorporating the long-range tail function

$$u_{LR}^{a^3\Sigma_u^+}(r) = D_6(r)\frac{C_6}{r^6} + D_8(r)\frac{C_8}{r^8} + D_{10}(r)\frac{C_{10}}{r^{10}}, \quad (38)$$

in which $D_{m_i}(r)$ are the modified Douketis-type damping functions of Eq. (13), with $s = -1$ and $\rho = 0.54$ [24], and the dispersion energy coefficients for this state were fixed at the values reported by Tang et al. [42].

In the initial work to determine an optimum model for this state, the PAS data for the $1^3\Sigma_g^+$ state were ignored and all of the observed levels of both the $1^3\Sigma_g^+$ and $2^3\Pi_g$ states were represented by independent term values, so only a single potential energy function was involved in the analysis. Fits were then performed to a wide variety of models corresponding to different choices for the order N of the polynomial in Eq. (14), and for the power q and the reference distance r_{ref} of Eq. (15). As was pointed out in Section 2.2, the power p must be larger than the difference between the largest and smallest powers of the terms contributing to Eq. (38), so it was fixed as $p = 5$.

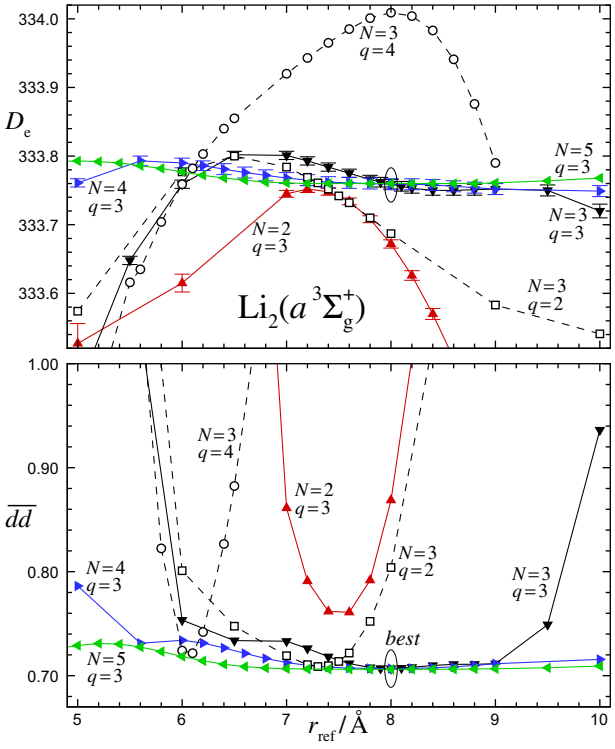

Fig. 5. Determination of the optimum model for the $a^3\Sigma_u^+$ state of Li_2. All energies are in cm^{-1}.

Fig. 5 summarizes results obtained for six families of potential function models of this type. In general we expect that for reasonable values of q (say, $2 \lesssim q \leqslant p$) and r_{ref} (say, $r_e \lesssim r_{ref} \lesssim 2r_e$), a good fit ($\overline{dd} \lesssim 1$) will always be achieved when the polynomial order N becomes sufficiently large. In the lower panel of Fig. 5, this behavior is seen in the convergence of the four families of solid triangular points that correspond to models with $q = 3$ as N increases from two to five. The results for $N = 3$ with $q = 2$ and 4 (open square and round points, respectively) show that the optimum value of r_{ref} (i.e., the one which gives the lowest $\overline{dd}$) will depend on q, but convergence to the same limiting quality-of-fit $\overline{dd}$. The upper panel of Fig. 5 shows the fitted values of $\mathfrak{D}_e$ for the various models considered in the lower panel. Those results show that the fitted value of $\mathfrak{D}_e$ may vary considerably from one model to another, but at the r_{ref} value where $\overline{dd}$ approaches its minimum value, all of the models with decent qualities of fit converge to essentially the same value.

All of the fits that are summarized by Fig. 5 used all of the 2692 'optical' data listed in Table 1 for the two isotopologues $^{7,7}Li_2$ and $^{6,6}Li_2$, plus the one PAS datum which had been reported for the $a^3\Sigma_u^+$ state, while the 395 term values of the observed levels of the $1^3\Sigma_g^+$ state and 20 term values for the $2^3\Pi_g$ state were treated as free parameters. As might be expected when dealing with light atoms such as Li, BOB effects are not negligible in this system. In particular, it was found that allowing for one non-zero term u_0^{Li} in the expression for the 'adiabatic' correction radial strength function of Eq. (27) reduced the value of $\overline{dd}$ by 2.4%; however, freeing a second coefficient (u_1^{Li}) only reduced $\overline{dd}$ by an additional 0.08%, and

Table 2
Parameters defining the recommended MLR potentials and BOB correction functions for the $a^3\Sigma_u^+$ and $1^3\Sigma_g^+$ states of Li_2 obtained using $^{7,7}Li_2$ as the reference isotopologue. Parameters in square brackets were held fixed in the fit, while numbers in round brackets are 95% confidence limit uncertainties in the last digits shown. The analysis used the $^7Li\ ^2P_{1/2} \leftarrow {}^2S_{1/2}$ excitation energy of $\frac{1}{\lambda_{SP}} = 14903.648130\ cm^{-1}$ and $^2P_{3/2} \leftarrow {}^2P_{1/2}$ spin-orbit splitting energy of $0.335338\ cm^{-1}$ from Ref. [38]. Units of length and energy are Å and cm^{-1}; the polynomial coefficients β_i are dimensionless, while the parameters u_i defining the 'adiabatic' BOB strength function of Eq. (27) have units cm^{-1}.

	$a^3\Sigma_u^+$		$1^3\Sigma_g^+$
$\mathfrak{D}_e$	333.758(7)		7093.44(3)
r_e	4.17005(3)		3.06514(9)
C_6	[6.7185×10^6][a]	C_3	$3.57557(78) \times 10^5$
C_8	[1.12629×10^8][a]	C_6^Σ	[1.00054×10^7][a]
C_{10}	[2.78683×10^9][a]	C_8^Σ	[3.69953×10^8][a]
ρ_{Li}	[0.54]		[∞][b]
{p,q}	{5, 3}		{6, 3}
r_{ref}	[8.0]		[3.6]
β_0	−0.51608		−1.6373863
β_1	−0.09782		0.29197
β_2	0.1137		−0.55544
β_3	−0.0248		−0.2794
β_4	–		−1.5993
β_5	–		−0.673
β_6	–		−1.23
β_7	–		−1.29
β_8	–		0.5
β_9	–		2.6
{p_{ad}, q_{ad}}	{6, 6}		{3, 3}
u_0	0.059 (11)		1.367(7)
u_1	–		2.7 (4)
u_2	–		−1.3(5)
u_3	–		−1.8(4)
u_∞	[0.0]		[1.055740]

[a] From Ref. [42].
[b] As explained at the end of the first paragraph of Section 3.3, setting $\rho = \infty$ in (13) effectively means that damping functions are not used.

the resulting value of u_1^{Li} had an uncertainty of greater than 100%. Similarly, allowing one centrifugal BOB parameter t_1^{Li} to vary led to reductions in $\overline{dd}$ of less that 0.05%. As a result, the model actually used to obtain the results summarized in Fig. 5 included only the one free BOB parameter u_0^{Li}.

All else being equal, the 'best' model for a given system is the one which achieves a good quality of fit (lowest $\overline{dd}$) with the smallest number of free parameters and has no unphysical behaviour in the extrapolation regions. When more than that minimum number of parameters are used, the additional degrees of freedom in parameter space will not be strongly constrained by the data, and the possibility of problems in the extrapolation regions tends to increase. On these bases we choose the M3LR$^{8.0}_{5.3}(3)$ model corresponding to the solid black triangle points at r_{ref} = 8.0 Å on Fig. 5 as our preferred model, whose quality of fit as defined by Eq. (2) is $\overline{dd} = 0.7069$. The analysis described above led to our estimate of optimal values for p, q, r_{ref} and N for the $a^3\Sigma_u^+$ state potential, and our estimate of an optimal number of terms for the BOB correction functions (27) and (28). These values were then used in the global two-state potential fit (discussed in Section 3.3), which simultaneously determined potential energy functions for both the $a^3\Sigma_u^+$ state and the $1^3\Sigma_g^+$ state, with all other $a^3\Sigma_u^+$ state parameters reoptimized, and all $1^3\Sigma_g^+$ state parameters optimized.

A final point here concerns the extrapolation properties of the MLR potential function form. In the initial stages of this study, only the optical $1^3\Sigma_g^+ - a^3\Sigma_u^+$ data which spanned vibrational levels $v(a^3\Sigma_u^+) = 0$–7 were considered in the analysis. The highest of these $a^3\Sigma_u^+$ state levels is bound by about 26 cm^{-1} (for the reference isotopologue ^{7,7}Li$_2$). Nonetheless, our MLR potential obtained from that analysis (chosen based on the criteria mentioned in the first sentence of the last paragraph), was a function whose well depth (for the reference isotopologue) of $\mathfrak{D}_e = 333.761(13)$ cm^{-1} is very close to the value 333.759(7) cm^{-1} yielded by the analysis of the full $a^3\Sigma_u^+$ state data set (see Table 2). Similarly, the $v(a^3\Sigma_u^+) = 10$ binding energy predicted by that potential (which was calculated based only on information from $(v(a^3\Sigma_u^+) = 0$–$7)$ was 0.4168 cm^{-1}, which is remarkably close to the measured PAS value [15] of 0.4160(±0.0013) cm^{-1}. Finding a discrepancy of only 0.003 cm^{-1} in the estimate of $\mathfrak{D}_e$ and an error of only 0.0008 cm^{-1} in the predicted binding energy of the $v(a^3\Sigma_u^+) = 10$ level over an extrapolation distance of about 25 cm^{-1} demonstrates quite good extrapolation behavior. Thus, a DPF analysis using an MLR potential with a good multi-term theoretical $u_{LR}(r)$ seems to be capable of yielding quite reliable extrapolations to predict the dissociation energy, the binding energy of the highest observed level, and likely also the number and energies of unobserved higher levels.

3.3. Model for $Li_2(1^3\Sigma_g^+)$ and results of the two-state potential fit analysis

Following the discussion of Section 2.3, the potential energy function for the $1^3\Sigma_g^+$ state of Li_2 was represented by an MLR potential whose long-range tail was defined by $u_{LR}(r)$ of Eq. (26). As usual, fits were performed using models corresponding to a variety of values of the exponent polynomial order N, of the reference distance r_{ref} of Eq. (15), and of the power q. Since the inverse-power terms contributing to $u_{LR}(r)$ have powers $m_i \in \{3, 6, 8\}$, the power p defining the radial variables $y_p^{eq}(r)$ and $y_p^{ref}(r)$ of Eqs. (9) and (15) was fixed at $p = 6$ (which satisfies the requirement that it has to be larger than $m_{last} - m_1 = 8 - 3$), and while C_6^Σ and C_8^Σ were held fixed at the theoretical values of Tang et al. [42], C_3^Σ was treated as a free parameter. All of these fits treated the full range of data listed in Table 1 for the $1^3\Sigma_g^+ - a^3\Sigma_u^+$ system, and while the potential for the $a^3\Sigma_u^+$ state was represented by the M3LR$^{8.0}_{5.3}(3)$ model described in Section 3.2, its parameters were also free variables in these fits.[7] Because of the added intricacy arising from the interstate coupling near the dissociation asymptote, damping functions were omitted from the current model for this state, although in principle they could have been added for a more physically realistic inner potential wall. For this state's potential, omitting damping functions means that all $D_{m_i}(r)$ factors which ordinarily would be multiplied by the corresponding C_{m_i} coefficients as shown in Eq. (12), are set to 1. This choice for the damping functions $D_{m_i}(r)$ can be considered as setting $\rho = \infty$ in (13).

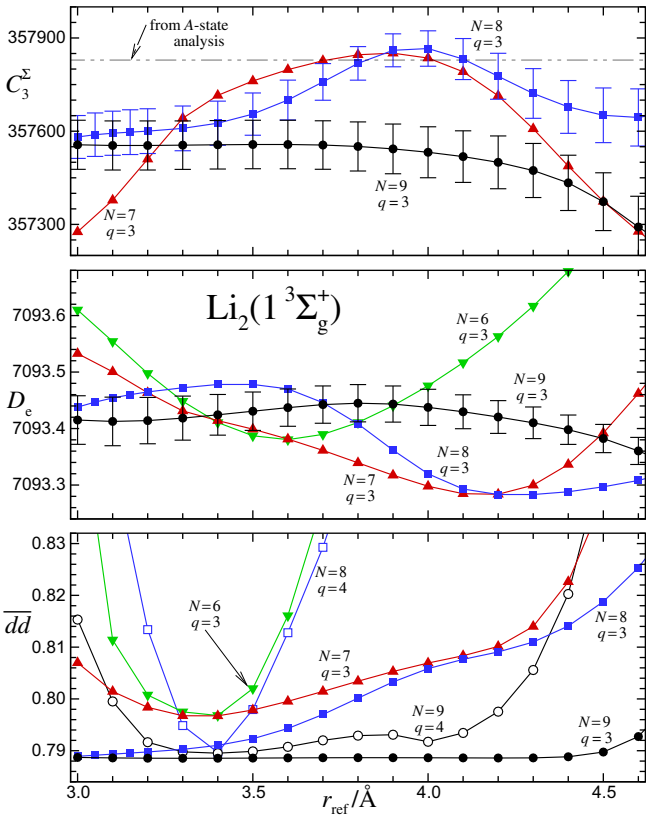

Fig. 6. Determination of the optimum model for the $1^3\Sigma_g^+$ state of Li_2. All energies are in cm^{-1} and lengths are in Å.

Fig. 6 summarizes results for six families of $1^3\Sigma_g^+$ state PECs: those for exponent polynomial orders N = 6–9 with q = 3 being represented by solid points, while those for polynomials orders N = 8–9 with q = 4 (bottom panel only) are shown as open points. As is expected, the fact that the 395 observed $1^3\Sigma_g^+$ state level energies are now constrained to be eigenvalues of a potential function rather than being free fitting parameters means that the $\overline{dd}$ values associated with the best of these fits are somewhat larger than those for the $a^3\Sigma_u^+$ state analyses summarized in Fig. 5.

As has been the case in other treatments of this type, for any reasonable values of q and r_{ref} the fits converge to essentially the same optimum $\overline{dd}$ value when the polynomial order N becomes sufficiently large [10,24,31,47]. A manual optimization of r_{ref} is undertaken in order to determine a 'best' model, which is defined as one which: (i) gives a good fit to all data, (ii) is defined by the smallest number of free parameters necessary, and (iii) has no unphysical behavior in the extrapolation regions. As is usually the case, models with larger q values (here q = 4) require a high-

[7] Although they were free parameters in the two-state fit, the resulting value of r_e was unchanged (to 6 decimal places), that of $\mathfrak{D}_e$ changed by only 0.001 cm^{-1}, and the largest change in a β_i coefficient was by 1.6%. Please see the Supplementary material for the full details.

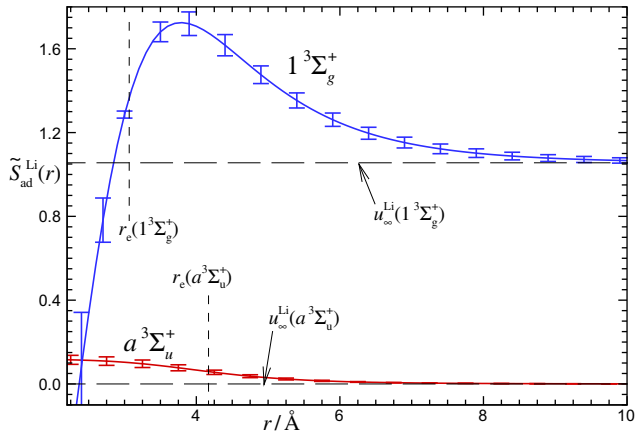

Fig. 7. BOB radial strength functions (in cm^{-1}) determined with $^{7,7}Li_2$ as the reference isotopologue.

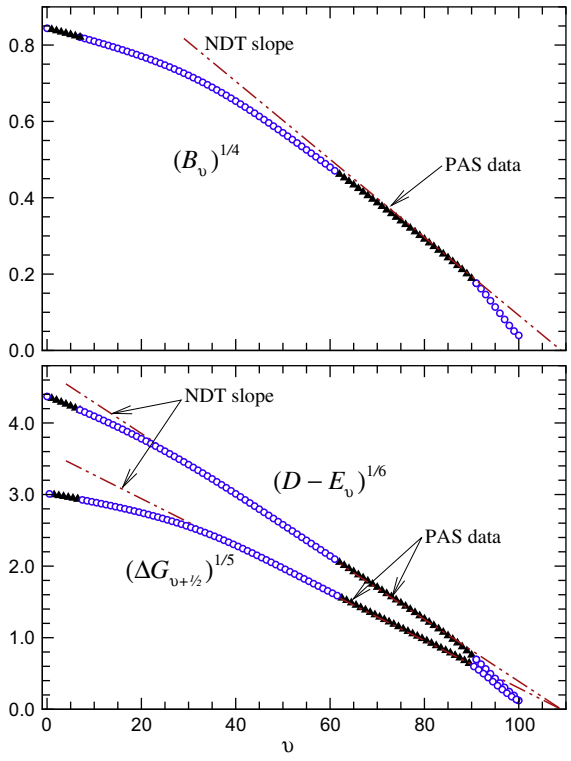

Fig. 8. Spectroscopic properties of the $1^3\Sigma_g^+$ state of $^{7,7}Li_2$.

er-order polynomial to achieve a given quality of fit. While not shown, the $\overline{dd}$ values for $N = 10$, $q = 4$ models with $r_{ref} = 3.4$–3.6 are essentially identical to those for $N = 9$, $q = 3$ models with the same r_{ref} (solid round points), but are bigger at larger and smaller r_{ref} values. Models with $q = 1$ or 2 tended to have inflection points on the short-range repulsive wall, even for cases with fairly large r_{ref} values.

The results in the two upper panels of Fig. 6 show that the values of $\mathfrak{D}_e$ and C_3^Σ yielded by fits to models with $N = 9$, $q = 3$ vary relatively slowly with r_{ref}, and that for r_{ref} values which give small $\overline{dd}$ values, different models yield similar results. For both of these properties the analogous results for $q = 4$ models were much more strongly model-dependent. We therefore favored the $N = 9$, $q = 3$ family of potentials over the others presented in that figure. Since the fitted C_3^Σ values and $\overline{dd}$ values seem to be more consistent for lower r_{ref} values than for higher ones, we also favored low r_{ref} values. Of the potentials that we fitted (see Fig. 6), the one of the family $N = 6$, $q = 3$ with the smallest r_{ref} value that did not have an inflection in the inner-wall extrapolation region, was the one with $r_{ref} = 3.6$ Å, hence we chose this case as our recommended model for this state.

The error bars shown in Fig. 6 are the 95% confidence limit uncertainties in the corresponding parameters yielded by the non-linear least-squares fits. Although the binding energies of the highest observed levels for the $1^3\Sigma_g^+$ state are even smaller than was the case for the $A^1\Sigma_u^+$ state [16], the uncertainties in the fitted C_3^Σ values obtained here ($\gtrsim 75$ cm^{-1}Å^3) are an order of magnitude larger than the analogous uncertainties yielded by the $A - X$ analysis of Ref. [10]. It is not clear why this should be the case, other than the fact that the data gap between $v(1^3\Sigma_g^+) = 7$ and 63 for $^{7,7}Li_2$ or between $v(1^3\Sigma_g^+) = 7$ and 56 for $^{6,6}Li_2$, may be expected to introduce additional uncertainty into the analysis of the limiting near-dissociation behavior. However, the difference between the C_3^Σ value implied by the present analysis and that determined from the A–X analysis of Ref. [10] (dash–dot–dot line in the uppermost panel of Fig. 6) is significantly larger than the mutual uncertainties. Moreover, repeating the present analysis with C_3^Σ fixed at the value yielded by the A–X analysis (357 829(±8) cm^{-1} Å^3) increased the overall value of $\overline{dd}$ by 0.8%, and increased the $\overline{dd}$ for the PAS data by a massive 21%! It may be that a combined 5-state analysis of the data sets for the two cases will resolve this discrepancy, but that is beyond the scope of the present work. Thus, our recommended model for the $1^3\Sigma_g^+$ state is an $M3LR^{3.6}_{6.3}(9)$ potential with $u_{LR}(r)$ defined by Eq. (26), and with C_3^Σ determined from the fit. The quality of this fit as defined by Eq. (2) is $\overline{dd} = 0.7888$.

The parameters defining our recommended models for the $a^3\Sigma_u^+$ and $1^3\Sigma_g^+$ states of Li_2 are listed in Table 2. The fact that the uncertainties in the values of $\mathfrak{D}_e$ and r_e are an order of magnitude larger for the $1^3\Sigma_g^+$ state is to be expected, both because of the gap of more than 5000 cm^{-1} for $7 < v(1^3\Sigma_g^+) < 63$, and because the fact that its lowest observed level is $v(1^3\Sigma_g^+) = 1$ means that the extrapolation to the potential minimum is much longer for this case. As for the $a^3\Sigma_u^+$ state, obtaining a good combined-isotopologue fit required the introduction of BOB corrections in the effective adiabatic potential function for the $1^3\Sigma_g^+$ state. As shown in Table 2, our recommended model includes a polynomial of degree three for the 'adiabatic' correction radial strength function $\widetilde{S}_{ad}^{Li}(r)$

Table 3
Properties of the recommended potential energy functions for the $a^3\Sigma_u^+$ and $1^3\Sigma_g^+$ states of Li_2 (energies in cm^{-1} and lengths in Å), with '*changes*' calculated using Eqs. (31)–(37). The first three rows correspond to use of $^{7,7}Li_2$ as the reference isotopologue, while for the last row it was $^{6,6}Li_2$. The numbers in brackets are 95% confidence limit uncertainties in the last digits shown.

		$a^3\Sigma_u^+$ *state*			$1^3\Sigma_g^+$ *state*			
fit	*isot.*	$\mathfrak{D}_e$	r_e	ΔT_e	$\mathfrak{D}_e$	$\mathfrak{D}_e^{tot}$	r_e	r_e^{tot}
2-*isot*	$^{7,7}Li_2$	333.758(7)	4.17005(3)	8144.989(43)	7093.44(3)	7092.417(33)	3.06514(9)	3.06524(9)
change		0.020(4)	−0.000012(3)	−0.265(5)	0.1036(3)	−0.067(2)	0.00005(3)	0.000075(1)
	$^{6,6}Li_2$	333.778(8)	4.170038(30)	8144.724(43)	7093.54(3)	7092.350(33)	3.06519(9)	3.065315(90)
2-*isot*	$^{6,6}Li_2$	333.778(7)	4.17001(3)	8144.726(33)	7093.54(3)	7092.347(33)	3.06520(9)	3.06532(9)

but no non-adiabatic centrifugal potential BOB correction function ($\widetilde{R}^{\rm Li}_{\rm na}(r)$). Increasing the degree of polynomial $\widetilde{S}^{\rm Li}_{\rm ad}(r)$ further or including a non-zero $\widetilde{R}^{\rm Li}_{\rm na}(r)$ yielded no significant improvement in the quality of fit as defined by Eq. (2), while reducing the degree of $\widetilde{S}^{\rm Li}_{\rm ad}(r)$ by one or two terms increased the $\overline{dd}$ value of the fit by 1.6% and 3.8%, respectively.

3.4. BOB functions and isotope effects

The radial strength functions defining the effective adiabatic BOB correction to the potential energy functions for both states are shown in Fig. 7. Since $^{7,7}Li_2$ was chosen as the reference isotopologue, Eq. (32) shows that the fact that $\widetilde{S}^{a^3\Sigma_u^+}_{\rm ad}\left(r_e^{a^3\Sigma_u^+}\right) - \widetilde{S}^{a^3\Sigma_u^+}_{\rm ad}(\infty) = u_0^{a^3\Sigma_u^+} - u_\infty^{a^3\Sigma_u^+} = u_0^{a^3\Sigma_u^+}$ is positive means that $\mathfrak{D}_e^{a^3\Sigma_u^+}$ is (slightly) larger for $^{6,6}Li_2$ than for $^{7,7}Li_2$. The upper curve in Fig. 7 shows that the $\widetilde{S}^{1^3\Sigma_g^+}_{\rm ad}(r)$ contribution to the isotopologue dependence of $\mathfrak{D}_e^{1^3\Sigma_g^+}$ is also positive (and much larger). However, the isotopologue dependence of the $2B^{(\alpha)}(r)$ contribution to the effective adiabatic potential (see Eq. (37)) makes a negative (-0.171 cm^{-1}) contribution to the difference $\mathfrak{D}_e^{\rm tot(6,6)} - \mathfrak{D}_e^{\rm tot(7,7)}$ for the $1^3\Sigma_g^+$ state, and turns out to be the dominant BOB correction term.

The results presented in Table 2 were obtained from an analysis which treated $^{7,7}Li_2$ as the reference isotopologue, and the first row of Table 3 presents characteristic properties of the resulting $a^3\Sigma_u^+$ and $1^3\Sigma_g^+$ potential energy functions for that species. Note that the values of $\mathfrak{D}_e^{\rm tot}(1^3\Sigma_g^+)$ and $r_e^{\rm tot}(1^3\Sigma_g^+)$ were obtained after combining the MLR potential with the additive adiabatic correction term of Eq. (36). The next two rows of this table then show, respectively, the isotopic changes in, and the resulting values of these quantities for $^{6,6}Li_2$, as implied by the BOB correction functions $\widetilde{S}_{\rm ad}(r)$ and (for the $1^3\Sigma_g^+$ state) the $2B^{(\alpha)}(r)$ term (see Eqs. (31)–(36)). Of course it is equally feasible to perform the overall analysis using $^{6,6}Li_2$ as the reference isotopologue, and the last row of Table 3 shows the properties of that isotopologue obtained in that more direct manner. It is reassuring to see that within the uncertainties, the results in the last two rows of this table agree with one another.

Of course it is simpler to work with potential functions that do not require the addition of separate adiabatic correction functions $\Delta V^{(\alpha)}_{\rm ad}(r)$. Hence, for the convenience of those interested primarily in the minor isotopologue $^{6,6}Li_2$, a version of Table 2 for the case in which this species was used as the reference isotopologue is included as Supplementary material.

4. Discussion and conclusions

A combined-isotopologue DPF analysis of 2692 optical data for the $1^3\Sigma_g^+ - a^3\Sigma_u^+$ and $2^3\Pi_g - a^3\Sigma_u^+$ band systems of $^{7,7}Li_2$ and $^{6,6}Li_2$, together with 99 PAS data for the $1^3\Sigma_g^+$ state and one for the $a^3\Sigma_u^+$ state, has yielded analytic potential energy functions for the $1^3\Sigma_g^+$ and $a^3\Sigma_u^+$ electronic states which (on average) explain all of those data within the experimental uncertainties ($\overline{dd} = 0.7888$). The resulting $a^3\Sigma_u^+$ state potential has only 4 empirical shape parameters ($\{\beta_i\}_{i=0}^{i=3}$) and accurately describes data spanning the whole potential well, including the very highest vibrational level of $^{7,7}Li_2$ which is bound by only about 0.4160 cm^{-1}. The resulting scattering lengths for $^{7,7}Li_2$ and $^{6,6}Li_2$ are $a_{\rm SL}$ = $-14.759(9)$ Å and $-1906(50)$ Å, respectively, where the uncertainties were estimated by repeating the overall analysis with $C_6^{a^3\Sigma_g^+}$ increased/decreased by 0.01% from the recommended values of Tang et al. [42]. This 0.01% is a factor of 3 larger than the C_6 uncertainty reported in Ref. [42]. The uncertainty in $a_{\rm SL}$ is much larger for $^{6,6}Li_2$ than for $^{7,7}Li_2$ simply because all else being equal, scattering lengths that are very large in magnitude are much more sensitive to details of the potential energy function. Listings of band constants (G_v, B_v, D_v, H_v, etc.) calculated from this potential for all bound levels of the $a^3\Sigma_u^+$ state for all three Li_2 isotopologues are included with the Supplementary material.

For the $1^3\Sigma_g^+$ state, the present analysis has provided an analytic potential energy function that smoothly bridges the gap of about 5000 cm^{-1} gap (see Fig. 1) between the $v(1^3\Sigma_g^+) = 1-7$ fluorescence measurement domain and the PAS data for $v(1^3\Sigma_g^+, ^{6,6}Li_2) \geqslant 56$ and $v(1^3\Sigma_g^+, ^{7,7}Li_2) \geqslant 63$. To illustrate this bridging behavior, Fig. 8 plots calculated properties of our recommended potential for $^{7,7}Li_2$ in the manner suggested by near-dissociation theory (NDT) [47–51]. In particular, NDT predicts that for vibrational levels lying near the dissociation limit of a potential whose limiting long-range behavior is defined by an attractive C_3/r^3 interaction energy, the $\frac{1}{6}$ power of the binding energy ($\mathfrak{D} - E_v$), the $\frac{1}{5}$ power of the vibrational level spacing $\Delta G_{v+\frac{1}{2}}$, and the $\frac{1}{4}$ power of the inertial rotational constant B_v, should all be linear functions of v, with slopes determined by the value of the C_3 coefficient. The solid triangular points in Fig. 8 represent the experimental data, while the open round points are our predictions for the 'no-data' regions. The markers (triangular points and open round points) will not exactly appear to represent vibrational levels with a 1:1 correspondence due to some overlaps. The dash–dot–dot lines in Fig. 8 are the limiting NDT slopes implied by the fitted C_3^Σ value of Table 2; as an NDT treatment was the basis of the analysis reported in Ref. [16], this plot suggests that it is fortunate that the data available there did not extend past $v(1^3\Sigma_g^+, ^{7,7}Li_2) = 90$. The deviation from the NDT behavior at very high v reflects the fact that the 3×3 interstate coupling reduces the magnitude of the effective C_3 coefficient in the limiting region by a factor of $\frac{1}{3}$ (a discussion regarding the asymptotic form of the potential is in the Supplementary materials) as one approaches the limit (see Fig. 4). Calculated band constants for all bound levels of all three Li_2 isotopologues in this state have been placed in the Supplementary material.

It is noteworthy that predictions generated from a variety of other MLR potential models (i.e., models defined by different N or q values) which yield good fits to the data are identical on the scale of Fig. 8. This model-independent bridging of a data-gap spanning 73% of the well depth is a remarkable illustration of the robustness of the MLR potential function form. The ability of this function to readily incorporate the effect of two-state [10] or three-state (present work) coupling in the long-range region is a further demonstration of its capabilities. A FORTRAN subroutine for generating the recommended potentials has been placed in the Supplementary material.

One puzzle left by this work is the discrepancy between the value of C_3^Σ for interacting Li(^2P)+Li(^2S) atoms determined in the present analysis ($3.57557(78) \times 10^5$ cm^{-1}Å^3) and those obtained in the $A(^1\Sigma_u^+)$ state analysis of Ref. [10] ($3.57829(7) \times 10^5$ cm^{-1}Å^3) or from the recent theoretical calculations of Tang et al. [42], ($3.5781089(7) \times 10^5$ cm^{-1}Å^3). While small on an absolute scale, this 0.076% discrepancy is much larger than the estimated uncertainties, and repeating our overall analysis with C_3^Σ fixed at the $A(^1\Sigma_u^+)$ state value from Ref. [10] yielded a distinctly poorer quality fit, especially for the PAS data. It may be that a combined five-state analysis of all of the data considered here with those used in the A–X analysis of Ref. [10] will shed light on this question, but that will have to await future work.

Acknowledgments

We are very grateful to Dr. Amanda Ross for stimulating discussions which brought this problem to our attention, and to Professor F.R.W. McCourt for helpful discussions. This research has been supported by the Natural Sciences and Engineering Research Council of Canada.

Appendix A. Supplementary material

Supplementary data for this article are available on ScienceDirect (www.sciencedirect.com) and as part of the Ohio State University Molecular Spectroscopy Archives (http://library.osu.edu/sites/msa/jmsa_hp.htm). Supplementary data associated with this article can be found, in the online version, at doi:10.1016/j.jms.2011.03.030.

References

[1] D.K. Hsu, The Absorption Spectra of the *A*–*X* and *C*–*X* Transitions of the ($^7Li_2$) Lithium Molecule, Ph.D. Dissertation, Fordham University, 1975.
[2] B. Barakat, R. Bacis, F. Carrot, S. Churassy, P. Crozet, F. Martin, J. Vergès, Chem. Phys. 102 (1986) 215.
[3] K. Urbanski, S. Antonova, A. Yiannopoulou, A.M. Lyyra, L. Li, W.C. Stwalley, J. Chem. Phys. 104 (1996) 2813. Erratum K. Urbanski, S. Antonova, A. Yiannopoulou, A.M. Lyyra, L. Li, W.C. Stwalley, J. Chem. Phys. 116 (2002) 10557.
[4] C. Linton, F. Martin, I. Russier, A.J. Ross, P. Crozet, S. Churassy, R. Bacis, J. Mol. Spectrosc. 175 (1996) 340.
[5] F. Martin, M. Aubert-Frécon, R. Bacis, P. Crozet, C. Linton, S. Magnier, A. Ross, I. Russier, Phys. Rev. A 55 (1997) 3458.
[6] X. Wang, J. Yang, J. Qi, A.M. Lyyra, J. Mol. Spectrosc. 191 (1998) 295.
[7] X. Wang, J. Magnes, A.M. Lyyra, A.J. Ross, F. Martin, P.M. Dove, R.J. Le Roy, J. Chem. Phys. 117 (2002) 9339.
[8] A. Adohi-Krou, F. Martin, A.J. Ross, C. Linton, R.J. Le Roy, J. Chem. Phys. 121 (2004) 6309.
[9] J.A. Coxon, T.C. Melville, J. Mol. Spectrosc. 235 (2006) 235.
[10] R.J. Le Roy, N. Dattani, J.A. Coxon, A.J. Ross, P. Crozet, C. Linton, J. Chem. Phys. 131 (2009) 204309.
[11] X. Xie, R.W. Field, J. Chem. Phys. 83 (1985) 6193.
[12] F. Martin, R. Bacis, J. Vergés, C. Linton, G. Bujin, C.H. Cheng, E. Stad, Spectrochim. Acta A 44 (1988) 1369.
[13] C. Linton, T.L. Murphy, F. Martin, R. Bacis, J. Verges, J. Chem. Phys. 91 (1989) 6036.
[14] C. Linton, F. Martin, A.J. Ross, I. Russier, P. Crozet, A. Yiannopoulou, L. Li, A.M. Lyyra, J. Mol. Spectrosc. 196 (1999) 20.
[15] E.R.I. Abraham, W.I. McAlexander, C.A. Sackett, R.G. Hulet, Phys. Rev. Lett. 74 (1995) 1315.
[16] E.R.I. Abraham, N.W.M. Ritchie, W.I. McAlexander, R.G. Hulet, J. Chem. Phys. 103 (1995) 7773.
[17] R.J. Le Roy, J. Seto, Y. Huang, `DPotFit 1.2`: A Computer Program for fitting Diatomic Molecule Spectra to Potential Energy Functions, University of Waterloo Chemical Physics Research Report CP-664,2007. <http://leroy.uwaterloo.ca/programs/>.
[18] R. J. Le Roy, `betaFIT 2.0`: A Computer Program to Fit Potential Function Points to Selected Analytic Functions, University of Waterloo Chemical Physics Research Report CP-665, 2009. <http://leroy.uwaterloo.ca/programs/>.
[19] J.K.G. Watson, J. Mol. Spectrosc. 80 (1980) 411.
[20] J.K.G. Watson, J. Mol. Spectrosc. 223 (2004) 39.
[21] R.J. Le Roy, J. Mol. Spectrosc. 194 (1999) 189.
[22] R.J. Le Roy, Y. Huang, J. Mol. Struct. (Theochem) 591 (2002) 175.
[23] Y. Huang, R.J. Le Roy, J. Chem. Phys. 119 (2003) 7398; . ErratumY. Huang, R.J. Le Roy, J. Chem. Phys. 126 (2007) 169904.
[24] R.J. Le Roy, C.C. Haugen, J. Tao, H. Li, Mol. Phys. 109 (2011) 435.
[25] H. Margenau, Rev. Mod. Phys. 11 (1939) 1.
[26] J.O. Hirschfelder, C.F. Curtiss, R.B. Bird, Molecular Theory of Gases and Liquids, Wiley, New York, 1964.
[27] J.O. Hirschfelder, W.J. Meath, in: J.O. Hirschfelder (Ed.), Intermolecular Forces, Advances in Chemical Physics, vol. 12, Interscience, New York, 1967, pp. 3–106 (Chapter 1).
[28] G.C. Maitland, M. Rigby, E.B. Smith, W.A. Wakeham, Intermolecular Forces-Their Origin and Determination, Oxford University Press, Oxford, UK, 1981.
[29] H. Kreek, W.J. Meath, J. Chem. Phys. 50 (1969) 2289.
[30] C. Douketis, G. Scoles, S. Marchetti, M. Zen, A.J. Thakkar, J. Chem. Phys. 76 (1982) 3057.
[31] J.A. Coxon, P.G. Hajigeorgiou, J. Chem. Phys. 132 (2010) 094105.
[32] R.J. Le Roy, Y. Huang, C. Jary, J. Chem. Phys. 125 (2006) 164310.
[33] R.J. Le Roy, R.D.E. Henderson, Mol. Phys. 105 (2007) 663.
[34] H. Salami, A.J. Ross, P. Crozet, W. Jastrzebski, P. Kowalczyk, R.J. Le Roy, J. Chem. Phys. 126 (2007) 194313.
[35] F. Xie, V.B. Sovkov, A.M. Lyyra, D. Li, S. Ingram, J. Bai, V.S. Ivanov, S. Magnier, L. Li, J. Chem. Phys. 130 (2009) 051102.
[36] M. Movre, G. Pichler, J. Phys. B: At. Mol. Phys. 10 (1977) 2631.
[37] M. Aubert-Frécon, G. Hadinger, S. Magnier, S. Rousseau, J. Mol. Spectrosc. 188 (1998) 182.
[38] C.J. Sansonetti, B. Richou, R. Engleman Jr., L.J. Radziemski, Phys. Rev. A 52 (1995) 2682.
[39] G. Cardano, Ars Magna (1545).
[40] J. Kopp, Int. J. Mod. Phys. C 19 (2008) 523. <http:arXiv:physics/0610206v3>.
[41] C.G.J. Jacobi, J. für die Reine und Angew. Math. 30 (1846) 51.
[42] L.-Y. Tang, Z.-C-. Yan, T.-Y. Shi, J.F. Babb, Phys. Rev. A 79 (2009) 062712.
[43] R. McLone, E. Power, Mathematica II (1964) 91.
[44] W.J. Meath, J. Chem. Phys. 48 (1968) 227.
[45] W.I. McAlexander, E.R.I. Abraham, R.G. Hulet, Phys. Rev. A 54 (1996) R5.
[46] F. Vogt, C. Grain, T. Nazarova, U. Sterr, F. Riehle, C. Lisdat, E. Tiemann, Eur. Phys. J. D 44 (2007) 73.
[47] R.J. Le Roy, Determining equilibrium structures and potential energy functions for diatomic molecules, in: J. Demaison, A.G. Csaszar (Eds.), Equilibrium Structures of Molecules, Taylor & Francis, London, 2010, pp. 168–211 (Chapter 6).
[48] R.J. Le Roy, R.B. Bernstein, Chem. Phys. Lett. 5 (1970) 42.
[49] R.J. Le Roy, R.B. Bernstein, J. Chem. Phys. 52 (1970) 3869.
[50] R.J. Le Roy, Can. J. Phys. 50 (1972) 953.
[51] R.J. Le Roy, in: M. Child (Ed.), Semiclassical Methods in Molecular Scattering and Spectroscopy, Series C-Mathematical and Physical Sciences, vol. 53, D. Reidel, Dordrecht, 1980, pp. 109–126.
[52] Victor J. Katz, A History of Mathematics an Introduction, third ed., Pearson Education, Inc., 2009, pp. 399–401.